

**A missing piece of the *Papio* puzzle: Gorongosa baboon phenostructure and their relationships with *Papio* species**

Felipe I. Martinez<sup>1\*</sup>, Cristian Capelli<sup>2</sup>, Maria J. Ferreira da Silva<sup>3,4</sup>, Vera Aldeias<sup>5,6</sup>, Zeresenay Alemseged<sup>7</sup>, William Archer<sup>6</sup>, Marion Bamford<sup>8</sup>, Dora Biro<sup>2</sup>, René Bobe<sup>5,9,10</sup>, David R. Braun<sup>11</sup>, Jörg M. Habermann<sup>5,9,12</sup>, Tina Lüdecke<sup>9,13</sup>, Hilário Madiquida<sup>14</sup>, Jacinto Mathe<sup>10</sup>, Enquye Negash<sup>11</sup>, Luis M. Paulo<sup>15</sup>, Maria Pinto<sup>15</sup>, Marc Stalmans<sup>10</sup>, Frederico Táta<sup>5,15</sup>, & Susana Carvalho<sup>5,9,10,16</sup>

<sup>1</sup>Pontificia Universidad Católica de Chile, Facultad de Ciencias Sociales, Programa de Antropología, Av. Vicuña Mackenna 4860, Macul, Santiago 7820436, Chile; <sup>2</sup>Department of Zoology, University of Oxford, UK; <sup>3</sup>Organisms and Environment Division, School of Biosciences, Cardiff University, Biomedical Sciences Building, Room C/5.15, Museum Avenue, Cardiff, CF10 3AX, Wales, UK; <sup>4</sup>CIBIO/InBio, Centro de Investigação em Biodiversidade e Recursos Genéticos, Universidade do Porto, Portugal; <sup>5</sup>ICArEHB-Interdisciplinary Center for Archaeology and Evolution of Human Behaviour, University of Algarve, Campus de Gambelas, 8005-139, Faro, Portugal; <sup>6</sup>Department of Human Evolution, Max Planck Institute for Evolutionary Anthropology, Leipzig, Germany; <sup>7</sup>Department of Organismal Biology & Anatomy, University of Chicago, USA; <sup>8</sup>Evolutionary Studies Institute, University of the Witwatersrand, South Africa; <sup>9</sup>Primate Models for Behavioural Evolution, University of Oxford, UK; <sup>10</sup>Gorongosa National Park, Sofala, Mozambique; <sup>11</sup>George Washington University, USA; <sup>12</sup>GeoZentrum Nordbayern, Friedrich-Alexander-Universität Erlangen-Nürnberg, Germany; <sup>13</sup>Senckenberg Biodiversity and Climate Research Centre, Germany; <sup>14</sup>Universidade Eduardo Mondlane, Maputo, Mozambique; <sup>15</sup>AESDA - Associação de Estudos Subterrâneos e Defesa do Ambiente, Portugal; <sup>16</sup>Centre for Functional Ecology, Coimbra University, Portugal.

**\* Corresponding author. E-mail address: [fmartinezl@uc.cl](mailto:fmartinezl@uc.cl) (F.I. Martínez)**

**Abstract:** Most authors recognize six baboon species: hamadryas (*Papio hamadryas*), Guinea (*Papio papio*), olive (*Papio anubis*), yellow (*Papio cynocephalus*), chacma (*Papio ursinus*), and Kinda

baboon (*Papio kindae*). However, there is still debate regarding their taxonomic status, phylogenetic relationships, and the amount of gene flow occurring between morphotypes. Here, we present ongoing research on baboon morphological diversity in Gorongosa National Park (GNP). GNP is located in central Mozambique, south of the Zambezi River, at the southern end of the East African Rift System. The park exhibits outstanding ecological diversity and hosts more than 200 baboon troops. GNP baboons have previously been classified as chacma baboons (*P. ursinus*). In accordance with this, two mtDNA samples from the park have been placed in the same mtDNA clade as the northern chacma baboons. However, GNP baboons exhibit morphological features common in yellow baboons (e.g., yellow fur color), suggesting that parapatric gene flow between chacma and yellow baboons might have occurred in the past or could be currently ongoing. We investigated the phenostructure of the Gorongosa baboons using two approaches: 1) description of external phenotypic features, such as coloration and body size, and 2) geometric morphometric analysis of 43 3D craniofacial landmarks on 11 specimens from Gorongosa compared to a pan-African sample of 352 baboons. The results show that Gorongosa baboons are intermediate between *P. cynocephalus* south and *P. ursinus griseipes*. The GNP baboon phenotype fits within a geographic clinal pattern of replacing allotaxa. We put forward the hypothesis of either past and/or ongoing hybridization between the gray-footed chacma and southern yellow baboons in Gorongosa or an isolation-by-distance scenario in which the GNP baboons are geographically and morphologically intermediate. These two scenarios are not mutually exclusive. We highlight the potential of baboons as a useful model to understand speciation and hybridization in early human evolution.

**Keywords:** Gorongosa National Park, *Papio cynocephalus*, *Papio ursinus griseipes*, phylogeography, hybridization, geometric morphometrics.

## 1. Introduction

Baboons (*Papio* spp.) are distributed across sub-Saharan Africa and a small part of the Arabian Peninsula. Five baboon morphotypes are usually recognized as full-rank phylogenetic species (Newman et al., 2004; Zinner et al., 2009; Keller et al., 2010; Kopp et al., 2015; see Figure 1): hamadryas (*Papio hamadryas*), Guinea (*Papio papio*), olive (*Papio anubis*), yellow (*Papio cynocephalus*), and chacma baboons (*Papio ursinus*). In the 2016 IUCN assessment, the Kinda baboon (*Papio kindae*), previously considered a subspecies of the yellow baboon (*Papio cynocephalus kindae*), was upgraded to full species status. However, there is still debate regarding the *species* status of baboon morphotypes, their phylogenetic relationships, and the amount of hybridization occurring between them. Several hybrid zones between baboon morphotypes have been identified (e.g., Awash River, Ethiopia, Phillips-Conroy and Jolly, 1986; Amboseli, Kenya, Samuels and Altmann, 1986; Kafue National Park, Zambia, Jolly et al., 2011), suggesting that gene flow has been the norm rather than the exception within the genus *Papio*. One supposed area of boundary between species is central Mozambique (Kingdon, 1997; Zinner et al., 2009), a region poorly investigated so far. In this paper, we focus on this area by providing the first morphological description of the baboons in Gorongosa National Park (GNP), located in central Mozambique, just a few kilometers away from the boundary between the yellow and chacma baboons (Figure 2).

The six-species taxonomy is based on the phylogenetic species concept (PSC; Cracraft, 1983; Jolly, 2001), which emphasizes diagnosable aspects of the phenotype and monophyly to distinguish between taxa. By contrast, under the biological species concept (BSC; Mayr, 1942, 1982; Dobzhansky, 1937), *Papio* morphotypes would be considered subspecies of a single polytypic species (Jolly, 1993). Several authors have asserted that the evidence of natural hybridization makes the BSC taxonomic nomenclature of subspecies more suitable for *Papio* morphotypes (Frost et al., 2003; Barrett and Henzi, 2008; Singleton et al., 2017). However, under

the BSC nomenclature, geographically-circumscribed diversity would be underappreciated, due in part to the limitations of the Linnaean system (Jolly, 2003; Burrell, 2009). In order to avoid this inconsistency between the PSC and BSC definitions, Jolly (2001) uses the term allotaxa (Grubb, 1999) to describe baboon variation. Jolly (2001) defines allotaxa as “phylogenetically close, but well-differentiated and diagnosable geographically replacing forms whose ranges do not overlap, but are either disjunct, adjoining, or separated by comparatively narrow zones in which characters are clinally distributed” (Jolly, 2001:193-194; see also the contribution by Clifford Jolly in this special issue).

It has long been recognized that *Papio* species are morphologically well-differentiated (Kingston, 1997) and parapatrically distributed (Jolly, 1993; 2001). This observation is mainly based on diagnostic features of the phenotype, such as fur color and texture, body build, skull morphology, or tail carriage. Populations located near contact zones often exhibit mixed characteristics, making them intermediate forms. For example, Ibean yellow baboons from Kenya and Somalia display physical characteristics from olive baboons (Jolly, 1993). Also according to Jolly (1993), yellow baboons from Zambia, Malawi, and northern Mozambique were mistakenly classified as chacma baboons in the past (*P. ursinus jubilaeus* and “dwarf chacma”; Jolly, 1993). In Zambia, the yellow baboons from Luangwa National Park are currently classified as *P. cynocephalus jubilaeus*, and their mitochondrial DNA (mtDNA) clade is found in baboons at the Senga Hills Forest Reserve in Malawi (Zinner et al., 2015). In north-central Mozambique, yellow baboons are sometimes referred as *P. cynocephalus jubilaeus*, *P. cynocephalus strepitus*, or simply *P. cynocephalus spp.*, which reflects the lack of taxonomic agreement at the subspecies level in this region (Zinner et al., 2015; Hill, 1970). Thus, it is often interpreted that the external morphological features defining *Papio* species change in a stepwise regional pattern. According to Jolly (2003), this pattern corresponds to geographically replacing allotaxa, with at least 18

diagnosable allotaxa exhibiting some but not all of the features used to define contiguous morphotypes (Jolly, 2003).

Previous morphometric studies have been able to characterize baboon morphotype differences in craniofacial shape and sexual dimorphism as related to size and allometric scaling (Leigh and Cheverud, 1991; Collard and O'Higgins, 2001; Singleton, 2002; Frost et al., 2003; Leigh, 2006; Singleton et al., 2017). There is agreement that most of the cranial shape variation seen in *Papio* is explained by allometric scaling, with only *P. kindae* departing from a common ontogenetic trajectory (Leigh, 2006; Singleton et al., 2017). In addition, *Papio* craniofacial variation across geography has been modeled as a continuous northwest-southeast cline (Frost et al., 2003; Dunn et al., 2013). Frost et al. (2003) found that geographic location explains 60% of the variation in craniofacial shape after correcting for size and sex. Dunn et al. (2013) corroborated this finding, but added an east to west pattern of increasing and then decreasing size (no evidence of a Bergmannian trend). In addition, their study could not find any correlation attributable to ecological factors between morphology and environmental variables such as temperature, humidity, precipitation, vegetation, and altitude, with the exception of a correlation between centroid size and precipitation standard deviation in olive baboons. Although ecological factors (food resources, seasonality) cannot be ruled out (Dunbar, 1990), the morphometric data seem to favor population history and isolation by distance as straightforward explanations to the above-mentioned continental trend in craniofacial variation (Frost et al., 2003; Dunn et al., 2013).

The *Papio* northwest-southeast phenotypic cline includes a break that creates a north-south dichotomy between *P. papio*, *P. hamadryas*, and *P. anubis* in the north and *P. cynocephalus*, *P. kindae*, and *P. ursinus* in the south (Frost et al., 2003; Jolly, 2003). The differences between north and south translate morphologically into northern morphotypes exhibiting a broader crania and face than the narrower midface of the southern morphotypes. Also, southern morphotypes

have a more downwardly flexed face relative to the braincase (increased klinorhynch), producing a taller midface (Frost et al., 2003; Singleton et al., 2017). This north-south dichotomy is also reflected in pelage features: “wavy, bushy shoulder manes and cheek tufts” in the north and “straight, silky mane hairs, untufted cheeks and light facial patches” in the south (Jolly, 2003:1046).

The genetic data are also consistent with the north/south division. One of the most complete phylogenetic analyses carried out for *Papio* sp. (Zinner et al., 2009, 2011, 2013, 2015) replicated the north-south dichotomy but also revealed discordances between mtDNA phylogeny and morphology. Zinner and collaborators (2009) analyzed mtDNA variation in 67 specimens at 53 sites and identified seven main mtDNA haplogroups (label A to G) divided into two major geographic clades—a southern clade, grouping together *P. ursinus*, *P. kindae*, and southern *P. cynocephalus* (A to B; Zinner et al., 2009), and a northern clade, including *P. hamadryas*, *P. papio*, *P. anubis*, and northern *P. cynocephalus* (haplogroups D to G). The mismatch between yellow baboon morphotype and mitochondrial grouping indicates that *P. cynocephalus* is paraphyletic. This suggests a complex evolutionary history with several episodes of gene flow leading to different degrees of introgressive hybridization (Zinner et al., 2009, Keller et al., 2010; Zinner et al., 2013).

Based on mtDNA data, southern *P. cynocephalus* are grouped into the same haplogroup (B) as the northern *P. ursinus*. Keller et al. (2010) further investigated the southern mtDNA subclades with an emphasis on geographically close areas and suggested that males from the *P. ursinus* morphotype introgressed the southern *P. cynocephalus* range from south to north. As a result of this process, the southern *P. cynocephalus* populations maintained their yellow baboon mtDNA but acquired a mixed or predominantly chacma morphotype (via nuclear swamping: Zinner et al., 2009; Burrell, 2009; Keller et al., 2010; Zinner et al., 2011a, 2011b). Although alternative

explanations could be drawn (such as lineage sorting), this scenario is in agreement with the female philopatry and male dispersal exhibited by *P. ursinus* and *P. cynocephalus* (Barrett and Henzi, 2008; Fischer et al., 2017). It also fits the pattern of mtDNA subclade paraphyly between the northern and southern *P. ursinus* and may explain the difficulty in assigning the baboons found in Malawi and northwestern Zambia (*P. c. (u.) jubilaeus*), and north-central Mozambique (*P. c. jubilaeus* and *P. c. strepitus*) to the described morphotypes (Jolly, 1993). In turn, it predicts a morphological cline between *P. ursinus griseipes* (grayfooted chacma) and southern *P. cynocephalus* (through regionally replacing allotaxa) and the occurrence of further hybridization in contact zones north to the Middle Zambezi River (see Jolly et al., 2011). *P. u. griseipes* exhibits lighter coat color, slightly smaller crania, and larger body size than *P. ursinus ursinus* (Burrell, 2009); its feet are gray, and its tail is longer (Burrell, 2009; Jolly, 1993). The distribution of the grayfooted chacma ranges from south-central Mozambique to the extreme north of South Africa, Zimbabwe, north Botswana, south Zambia, a small portion of the extreme southeast of Angola, a small portion of the extreme northeast of Namibia (see Sithaldeen et al., 2009), including the Caprivi strip (Figure 1). According to Zinner et al. (2009) and Keller et al. (2010), the distribution of the northern chacma subclade most likely coincides with the subspecies *P. ursinus griseipes* (grayfooted chacma).

In Mozambique, the Lower Zambezi River is considered a biogeographic barrier between *P. cynocephalus* and *P. ursinus* (Kingdon, 1997). However, *P. u. griseipes* populations extend north over the Upper or Middle Zambezi River to the northeast and hybridize with *P. kindae* in the Kafue Valley in Zambia (Jolly et al., 2011). In fact, Jolly et al. (2011) found groups with individuals carrying mtDNA and Y chromosomes from both the Kinda and grayfooted chacma baboons, suggesting hybridization between these two parental species. Jolly and collaborators (2011) also studied phenotypic features exhibited in hybrid individuals, detecting troops with different degrees of

genetic admixture and intermediate morphotypes. In addition to this, *P. u. griseipes* populations are in contact with *P. cynocephalus* in the lower Luangwa Valley in Zambia (Burrell, 2009). Although unclear how far east this contact persists, Burrell (2009) argues the contact likely extends, north of the Zambezi, to the Indian Ocean in the Mozambican coast.

In this study, we set out to place the morphological variation of the baboon population in Gorongosa National Park, Mozambique within the context of broader regional diversity. The Gorongosa baboons were identified as chacma baboons in an earlier study (Tinley, 1977) and were more recently placed within the geographic range of northern chacma mtDNA clade (Zinner et al., 2009; Keller et al., 2010; see Figure 2). However, the Gorongosa baboons exhibit some features common to the yellow baboon, such as yellow fur, lightly-colored ventral hair, pink infraorbital skin, and other features frequently seen in the grayfooted chacma baboon, such as robust male body build, bent tail carriage, or downwardly flexed facial orientation (Figures 3 and 4). These observations lead to the hypothesis that parapatric gene flow between the grayfooted chacma and southern yellow baboons might have occurred in the past or could be currently ongoing in the GNP (Napier, 1981; Freedman, 1963; Booth and Freedman, 1970).

Documenting hybridization in grayfooted chacma baboons and the observed *phenostructure* of Gorongosa baboon troops is an interesting way to further explore baboon morphological diversity. The *phenostructure* corresponds to the information about the distribution of heritable traits, functionally intertwined with information about interbreeding or *zygostructure* (Jolly, 1993; 2003). We first describe the external phenotype of the Gorongosa baboon as compared to *P. u. griseipes*, *P. u. ursinus*, typical *P. cynocephalus*, and *P. kindae*. Second, we comparatively analyze Gorongosa baboon craniofacial morphology by means of geometric morphometric tools and place it within the broader context of *Papio* variation.



## 2. Materials and methods

### 2.1. Study area

Gorongosa National Park (GNP, total area 3,770 km<sup>2</sup>) is located in the central/northern part of Mozambique. GNP is bordered to the south by the Pungue River and to the north by the Nhandue River. GNP is located 100 km south of the Zambezi River, a major hydrological feature of the African continent. The park exhibits outstanding biodiversity, with habitats spanning from tall evergreen forests inside limestone gorges to miombo woodlands, to grassy *Acacia* woodlands, tall open *Combretum* woodlands, open floodplain grasslands, and seasonally flooded grasslands.

### 2.2. Observation of external phenotypic features

In order to evaluate the degree of morphological variation in GNP baboons, we qualitatively listed the phenotypic characteristics observed in baboons during field work and from field-recorded visual material (photographs and videos). The field season at GNP spanned six weeks, on average, during July-August 2016 and 2017. We used the following techniques to record video, take photographs, and complete observations: a) systematic follows of non-habituated groups in woodlands, b) surveys across the floodplain and woodlands, and c) close-proximity observations of human-habituated groups at Chitengo Camp.

We listed 14 phenotypic Gorongosa baboon features related to coloration and body size/shape (general fur color, color of dorsal hair, color of ventral hair, color of limbs, eyelid skin color, circum-orbital skin color, hand/foot hair color, presence of silvery fringe on hands/feet, male body build, degree of sexual dimorphism, tail shape, facial orientation, natal coat color, infant stage two hair color; see Table 1). We compared these characteristics to the yellow, Kinda, grayfooted chacma, and southern chacma baboon features described in the literature (Altmann et al., 1981; Jolly et al., 2011; Alberts et al., 2001; Jolly, 1993; Swedell et al., 2011;

<http://kennychiou.com>). Infant stage two (estimated age 8 to 18 months) was defined according to Altmann et al. (1981).

### 2.3. Morphometric sampling and data acquisition

The sample for morphometric analysis comprises 363 cranial specimens (homologous 3D landmark configurations representing the baboons' craniofacial skeleton). Table 2 shows the composition of the morphotypes pursuant to sex and sample size. Our sample combines coordinate data obtained from two different sources. Three hundred and fifty-five specimens correspond to manually digitized coordinates obtained from an earlier study conducted by Dunn et al. (2013). In their database, specimens are grouped into one of the six species taxonomies, with one subspecies labeling for four individuals (*P. ursinus griseipes*). The database also included 318 geo-referenced specimens (274 geo-referenced specimens intersect with the 355 specimens labeled by species and sex). We subdivided *P. cynocephalus* into three subgroups by their geographic location: *P. cynocephalus* north (specimens located north of the Ruaha-Rufiji River in Central Tanzania; Zinner et al., 2015), *P. cynocephalus* south (specimens located south of the Ruaha-Rufiji River) and *P. cynocephalus* DRC (specimens located in the southern part of the Democratic Republic of Congo, labeled Zaire in the database), which is included in the distribution area of Kinda baboons. Two specimens labeled as *P. ursinus* and one specimen labeled as *P. cynocephalus* had geographic coordinates locating their origin in Gorongosa.

Specimens were divided into 10 groups, taking into account the six-species scheme, the subspecies *P. ursinus griseipes*, the paraphyly of *P. cynocephalus* (grouping yellow baboons according to geographic location), and considering Gorongosa as an independent group.

We added eight baboon skulls collected in Gorongosa National Park during the 2016 and 2017 field work to the database. The skulls were from naturally deceased and taphonomically-

skeletonized individuals. The skulls were surface-scanned in three different views using a NextEngine Desktop 3D Scanner from NextEngine, Inc., operating with both laser and normal light. Each view was a 360° scan with 11 divisions. The geometric point resolution was set to 66 dots per inch (DPI). ScanStudio 2.0.2 software (NextEngine, Inc., 2006) was used to merge the view scans into a single-surface model. Sholts et al. (2011) evaluated the precision of surface models generated by the Next Engine Scanner. Although well-recognized that manually-digitized measurements exhibit better overall precision, surfaces obtained with the Next Engine Scanner are suitable for craniometric research and are comparable to digitized coordinates (Sholts et al., 2011). Surface models were imported into the Amira 5.5 software (Mercury Inc. USA). A set of 43 three-dimensional landmarks was digitized on each baboon craniofacial surface model (see Table 3 for anatomical landmark description). The same 43 landmarks were extracted from the original Dunn et al. (2013) database. We selected type I and II landmarks (Bookstein, 1991) to circumvent the differences in measurement error between coordinates obtained with digitizers and the 3D models.

#### *2.4. Geometric morphometric analysis*

Routine geometric morphometrics procedures were used to analyze landmark configurations data. We performed Generalized Procrustes analysis (GPA) superimposition, minimizing the sum of square Euclidian distances between corresponding landmarks; scaling was done using unit centroid size (Bookstein, 1991; Slice, 2001). Principal component analysis (PCA) was used to visualize sample distributions by projecting the multidimensional Procrustes coordinates into a Euclidian tangent space. The PCA ordination makes no assumption about data classification. Rather, it is meant to explore trends by reducing dimensionality into a set of orthogonal (uncorrelated) components (PC). We run the overall PCA on all specimens (males and

females together) in order to explore the general trend in the entire sample. In the following analyzes, we treated males and females independently.

As mentioned in the introduction, previous studies have characterized the pattern of craniofacial shape change in relation to size in baboons (Leigh and Cheverud, 1991; Collard and O'Higgins, 2001; Singleton, 2002; Frost et al., 2003; Leigh, 2006; Dunn et al., 2013; Singleton et al., 2017). Here, as a means to investigate the pattern of shape variation that is not related to changes in size, we performed multivariate regression of shape on natural log-transformed centroid size (pooled by species/subspecies groups), for males and females independently. We obtained a "shape score" vector representing the strongest association with the size. Multiple permutation tests (1,000 rounds) were performed against the null hypothesis of independence between dependent (shape) and independent (size) variables. Residuals from the multivariate regression were treated as "size-corrected" shape coordinates (Drake and Klingenberg, 2008; Klingenberg and Marugan-Lobon, 2013).

Canonical variates analysis (CVA), discriminant function analysis (DFA), and between-groups PCA ordination were used to investigate the extent to which groups differed from one another. In order to account for unequal group size, we performed DFA for pairs of groups by leave-one-out cross-validations using 1000 permutation rounds (Klingenberg and Monteiro, 2005). To test the reliability of CVA ordinations, we performed between-groups PCA ordination (Mitteroecker and Bookstein, 2011). We calculated the mean configuration via GPA for each of the ten groups: *P. anubis*, *P. cynocephalus* north, *P. cynocephalus* south, *P. cynocephalus* DRC, *P. hamadryas*, *P. kindae*, *P. papio*, *P. ursinus*, *P. ursinus griseipes*, and Gorongosa. The CVA, DFA, and between-groups PCA were performed for males and females independently. Female CVA and DFA did not include *P. papio* (n = 1) and *P. cynocephalus* south (n = 2) due to low sample size, and *P. ursinus griseipes* due to lack of cases. Female between-groups PCA ordination did not include *P.*

*papio* and *P. ursinus griseipes*. All of the procedures were performed using MorphoJ version 1.06d (Klingenberg, 2008). Scatterplots were computed in R (<http://www.R-project.org/>).

Finally, we subjected the group mean configurations to a new GPA and computed dendrograms for morphological affinity using UPGMA and Ward's method as recommended for morphometric data (Hammer and Harper, 2008; Püschel et al., 2017). Euclidean distances were used as a similarity index. All principal components were used to compute the dendrograms in Past 3.18 software. In order to control for scanning error, we also computed comparative trees excluding the principal component (PC3) that summarized the most differences between the Gorongosa consensus and all other mean configurations in males and females.

## 2.5. Mantel correlograms

In order to evaluate the strength of the population history signal in our morphometric dataset, we compared the geographic pattern of phenetic autocorrelation in our data to an empirical model of genetic autocorrelation. To do so, we used Mantel correlograms pursuant to Le Boulengé et al. (1996), Borcard and Legendre (2012), and Diniz-Filho et al. (2013). Mantel correlograms are an extension of the Mantel test. Although the use of Mantel tests in ecology and evolutionary biology has recently been criticized (see Guillot and Rousset, 2013), Mantel correlograms have acceptable power in the absence of equivalent methods for assessing multivariate spatial correlation (Borcard and Legendre, 2012; Legendre et al., 2015). Mantel correlograms evaluate the spatial autocorrelation at different distance classes, computing a correlogram for multivariate data using the Mantel statistic ( $r_M$ ) for each distance class (Legendre and Legendre, 1998). Each distance class included all pairs of points located at a specific distance range from each other. Thus, a correlation index is calculated for each distance class. In our

implementation, we used specimen distances instead of population distances. This has two advantages. Firstly, our autocorrelation analysis is blind in relation to species, subspecies, morphotypes, or any group designation, preventing the bias that could result from species misidentification. Second, it increases sample size in order to assure that enough pairs of specimens within a given distance class are compared, which provides a reliable estimate for each rM class. The number of distance classes was set to six in both correlograms in order to reflect distance intervals closer to 1,000 km (1,109 km for the genetic correlogram, 1,153 km for the overall phenetic correlogram, 1,141 km for the male phenetic correlogram, and 1,125 km for the female phenetic correlogram). The statistical significance of each distance class was tested by setting 999 permutations. The progressive Bonferroni correction was used to account for multiple testing (Legendre and Legendre, 1998).

Phenetic autocorrelation was computed as morphological distances bounded within non-overlapping intervals of geographic distances. This was computed for the geo-referenced dataset (n=326), and separate males (n=241) and females (n=84). Note one sample was excluded for lack of information on sex. The morphological distances correspond to craniofacial shape distance matrices for each specimen (n=326) calculated based on the Procrustes shape coordinates, centroid size, and "size-corrected" shape residuals. The geographic distance matrix was calculated in km, computing geodesic distances from the geographic coordinates available for each specimen. Similarly, genetic autocorrelation was computed as genetic distances bounded within non-overlapping intervals of geographic distances. Genetic distances were computed as pairwise distances from a set of publicly available mitochondrial cytochrome b (CYT-B) gene sequences (Zinner et al., 2009; Keller et al., 2010). The sequences (n=153; 1,140 base pairs) were geo-referenced and a geodesic distance matrix was calculated in km. Genetic pairwise distances were computed after performing a likelihood ratio test to decide on the best-fit model for nucleotide

evolution. Distance matrices and Mantel correlograms were computed in R (<http://www.R-project.org/>) using the following packages: ade4 (Dray and Dufour, 2007), ape (Paradis et al., 2004), fossil (Vavrek, 2011), mpmcorrelogram (Matesanz et al., 2011), phangorn (Schliep, 2011), and vegan (Oksanen et al., 2018).

## 2.6. Surface warping

In order to visualize the trend in shape differences across groups, we computed targeted surface warpings. We obtained a warped surface for the consensus of each PCA ordination by warping one scanned specimen from Gorongosa (No. 34) using the Amira 5.5 software (Mercury Inc. USA) and the Bookstein spline interpolation method (Stalling et al., 2005). In order to represent female morphology, we followed a similar procedure using a surface obtained from Morphosource (<http://morphosource.org/>) an online repository of 3D scan data (Copes et al., 2016). This ply surface model corresponds to *P. kindae* specimen with catalog number NHMUK-ZD-1961.776 from the Natural History Museum, London. From each consensus, we targeted warped-surfaces along the principal components using the Evan toolbox (v.1.52, by the European Virtual Anthropology Network-Society [www.evan-society.org](http://www.evan-society.org)).

### 3. Results

#### 3.1. External phenotypic features of the Gorongosa baboon

We compared the phenotypic features of the Gorongosa baboon related to coloration and body size and shape. Specifically, we looked at the following traits: general fur color, dorsal coat color, ventral hair color, limb color, eyelid skin color, circum-orbital skin color, hand/foot hair color, presence of silvery fringe on hands/feet, male body build, degree of sexual dimorphism, tail shape, facial orientation, natal coat color, and infant stage two hair color; see Table 1 and Figures 3, 4 and 5.

The GNP baboons exhibit unusual phenotypic diversity, combining some features of the yellow baboon (yellow hair, light ventral hair, pink circum-orbital skin; also large male body size as *P. c. jubilaeus*, or silvery fringes in hands and feet as *P. c. strepitus*), and Kinda baboon (yellow hair, light ventral hair, pink circum-orbital skin, high-arched tail carriage) with others from the grayfooted chacma baboon (gray-brown hair, large body size, downwardly flexed face). The GNP baboon fur coloration generally varies between yellow-brown and gray-brown, and is paler ventrally, with white inner surfaces of limbs and lateral white patches on the muzzle between the eyes and the nostrils (Figures 3a-j). Their hind limbs tend to be paler (yellow) than their fore limbs (yellow-brown). The face is black and the skin around the callosities gray. They have pink eyelid skin (3d), and some individuals exhibit pink infraorbital skin (Figures 3e, 3f). The facial skeleton points downward (Figures 3g-3j, and Figure 5b) and the tip of the nose points forward in some females (Figure 3a). In occasions, females have a nuchal crest of longer flank hairs.

Adult males have no mane. They have elongated hair tufts along the nape (Figures 3g and 5b), and some show wavy, dark and bright stripes of hair on the back with long leg hair (Figure 3f). Sexual dimorphism is considerable (Figures 3i, 3j), and sexes seem to show variation in color (i.e., bigger males are darker gray-brown and females are paler yellow-brown). We observed some



adult males with yellow fur and sometimes a slenderer body build (Figure 3h). In most individuals, the color of the hands and feet is similar to their corresponding limbs but darker hands and feet were observed in some individuals (Figure 3e,i). Furthermore, some, but not all, individuals display a silvery fringe on the hands and feet (Figure 3d,f). Both, curved and bent/broken tails are present in the population. In broken tails, one-fourth of the tail ascends before descending sharply as if broken, like in the chacma (Figure 5c). Sometimes, the tail has two breaks (Figures 3g, 3h), although this feature could be due to life history events, such as fights and wounds. Observed females have a curved tail, sometimes with high-arched tail carriage (Figure 3i). The natal coat of infants is black and turns completely yellow at infant stage-2; black spots on the tail and head are the last to turn yellow (Figures 3a-3c).

### 3.2 Principal component analysis before size-correction

We explored the distribution pattern of the morphometric data using PCA before correcting for centroid size (Figure 6). Principal component 1 explains the largest amount of variation (45.6%), which is more than four times the variance explained by principal component 2 (9.9%). As expected, the variation summarized by PC1 is highly correlated with log-transformed centroid size ( $R^2 = 0.9$ ;  $P \text{ value} < 0.0001$ ) and related to sexual dimorphism ( $t\text{-statistics} = 15.21$ ;  $df = 361$ ;  $P \text{ value} < 0.0001$ ). The PC1 differentiates between male and female almost irrespective of species grouping, and shows the degree of sexual dimorphism present in *Papio*. The shape changes along the PC1 correspond to an increase in the projection of the face relative to the braincase (Figure 6; PC1, left side of the distribution), and a decrease in the projection of the face relative to the braincase (Figure 6; PC1, right side of the distribution). The shape changes along the PC2 correspond to an increase in klinorhynch (downwardly flexed face; Figure 6, PC2, down side of the distribution) and a decrease in klinorhynch (Figure 6; PC2, upper side of the distribution).

The PC1-PC2 scatterplot (Figure 6) show the distribution of species along a continuum. Larger species, such as *P. ursinus*, *P. anubis* and *P. cynocephalus* (north and south), tend to concentrate towards the left side of the distribution, whereas the medium-sized *P. papio* and *P. hamadryas* are intermediate. The smaller *P. kindae* falls together with specimens labelled as *P. cynocephalus* from DRC at the right side of the distribution. Two outliers may correspond to juvenile individuals but that information was not available in the dataset.

### 3.3 Multivariate regression on size

We performed pooled-within-groups multivariate regression of Procrustes coordinates on natural log-transformed centroid size (Klingenberg, 2008; Drake and Klingenberg, 2008). The resulting regression score represents the strongest association between shape and size (regression score 1) and accounts for 30.1% of the predicted variance (males = 10.5%; females = 14.3%; P value <0.0001). Figures 7a (males) and 7b (females) shows the distribution of groups along the allometric scaling relationship, which replicates the pattern of group distribution seen along PC1 (i.e., the larger species *P. ursinus*, *P. anubis* and *P. cynocephalus* north and south are clustered on one side of the distribution, the medium-sized *P. papio* and *P. hamadryas* are intermediate, and the smaller *P. kindae* falls together with *P. cynocephalus* DRC on the opposite side).

To investigate the patterns of shape variation unrelated to changes in size, we computed the residuals from the pooled-within-groups multivariate regression of Procrustes coordinates on natural log-transformed centroid size. We treated the residuals as "size-corrected" shape coordinates (Frost et al., 2003) in the following analyses.

### 3.4 Canonical variates and discriminant function analyses before and after size correction

We performed canonical variates analysis (CVA; Figures 8a and 8b) and discriminant function analysis (DFA; Tables 4, 5, 6 and 7) on Procrustes shape coordinates and "size-corrected" shape coordinates in order to evaluate differences between groups before and after correcting for size. Male DFA before size correction was unable to differentiate between Gorongosa/*P. ursinus griseipes*, *P. ursinus*/*P. ursinus griseipes*, *P. cynocephalus* south/*P. ursinus griseipes*, *P. cynocephalus* south/*P. ursinus*, *P. cynocephalus* south/*P. cynocephalus* north, and *P. kindae*/*P. cynocephalus* DRC (Table 4). Female DFA before size correction was unable to differentiate between Gorongosa/*P. ursinus*, *P. ursinus*/*P. hamadryas*, *P. hamadryas*/*P. cynocephalus* north, and *P. kindae*/*P. cynocephalus* DRC (Table 5). Male DFA on "size corrected" shape maintained similar results but was also unable to differentiate the *P. cynocephalus* north/ *P. ursinus griseipes* pair (Table 6). Female DFA on "size corrected" shape maintained undifferentiated the Gorongosa/*P. ursinus* and *P. kindae*/*P. cynocephalus* DRC pairs, and also *P. hamadryas*/*P. cynocephalus* north and *P. hamadryas*/*P. anubis* (Table 7). From these pairs of undifferentiated groups, we were interested in confirming *P. cynocephalus* south/ *P. u. griseipes*. In spite of small group sizes, DFA cross-validations shows difficulties in allocating *P. cynocephalus* south/ *P. u. griseipes* before and after correcting for size (Table 8; the reliability of the discrimination is assessed by leave-one-out cross-validation).

Figures 8a and 8b show the male and female CVA plots of "size-corrected" shape coordinates (similar results were obtained before size correction). For male CVA (Figure 8a; CV1=30%; CV2=22%), the GNP baboons are at one end of the distribution, overlapping with *P. ursinus*. The *P. kindae* and *P. cynocephalus* DRC groups cluster together. Besides *P. papio* and *P. kindae*/*P. cynocephalus* DRC, all of the other groups are distributed along a continuum. *P. anubis* is intermediate between *P. hamadryas* and *P. cynocephalus*, whereas *P. ursinus* encompasses all *P. ursinus griseipes* and most of *P. cynocephalus* south. A few *P. cynocephalus* north and south

individuals are actually closer to the *P. kindae*/*P. cynocephalus* DRC cluster. For female CVA (Figure 8b), the CV1 (53.8%) separates *P. kindae* and *P. cynocephalus* DRC from the rest. The separation is greater than the separation observed in the male CVA (Figure 8a). This is most likely due to the absence of *P. papio* in female CVA (Figure 8b). Along the CV2 (16.2%), the GNP baboons are grouped closer to *P. ursinus*. Interestingly, if we contrast the proximity of all groups to the *P. kindae*/*P. cynocephalus* DRC cluster along the CV1 (53.8%), the GNP baboons is the only group that deviates from the cluster conformed by *P. hamadryas*, *P. cynocephalus* north, *P. anubis*, and *P. ursinus*. This could suggest some sort of low degree of proximity between the female GNP baboons and the *P. kindae*/*P. cynocephalus* DRC cluster.

### 3.5 PCA of averaged groups and agglomerative-hierarchical cluster analysis

In order to visualize similarities across groups in the shape component not related to size, we calculated the mean configuration of each group (for males: *P. anubis*, *P. cynocephalus* north, *P. cynocephalus* south, *P. cynocephalus* DRC, *P. hamadryas*, *P. kindae*, *P. papio*, *P. ursinus*, *P. ursinus griseipes*, and Gorongosa; for females: *P. anubis*, *P. cynocephalus* north, *P. cynocephalus* south, *P. cynocephalus* DRC, *P. hamadryas*, *P. kindae*, *P. ursinus*, and Gorongosa) from the "size-corrected" shape residuals via GPA. Then, we subjected the mean configurations to a new GPA and plotted the main components (Figures 9a and 9b). For males (Figure 9a), PC1 summarizes 49.9% of the explained variance and represents shape changes related to klinorhynch. PC2 explains 21.5% and represents shape changes related to the breadth of the middle face. The distribution of the mean configurations shows that Gorongosa baboons are closer to *P. ursinus*, *P. ursinus griseipes*, and *P. cynocephalus* south, while *P. cynocephalus* north, *P. anubis*, *P. hamadryas*, and *P. papio* form a more loose-fitting cluster. *P. kindae* falls closer to *P. cynocephalus* DRC, and both are apart from other group means. For females (Figure 9b), PC1 summarizes 48.1% of the

explained variance and PC2 explains 21.4%. PC1 represents shape changes related to the elongation of the face; PC2 represents shape changes related to the breadth of the middle face (Figure 9b). The distribution of the mean configurations shows that Gorongosa baboons fall between *P. ursinus* and *P. cynocephalus* south (Figure 9b). *P. cynocephalus* north, *P. anubis*, *P. hamadryas*, and *P. papio* form a more loose-fitting cluster. *P. kindae* falls closer to *P. cynocephalus* DRC, and both are apart from other group means. The lower components for male and female between-groups PCA are shown in Figure 10 (a-g).

In order to locate Gorongosa baboons within the craniofacial variability of the genus *Papio*, we performed a cluster analysis using the unweighted pair-group method with arithmetic mean (UPGMA) and Ward's method (Hammer and Harper, 2008; Püschel et al., 2017). We computed a pairwise Euclidean distances matrix from the mean group "size-corrected" PC scores. The resulting phenogram trees (Figures 11 and 12) show the overall similarities across mean groups by creating dichotomous relations among the branches.

For males, the first UPGMA tree (Figure 11a) shows a dichotomy between the southern and northern baboons. The northern branch clusters *P. anubis* and *P. cynocephalus* north, *P. hamadryas*, and then *P. papio*. The southern branch clusters *P. ursinus* and *P. ursinus griseipes*, and then *P. cynocephalus* south. Gorongosa falls within this southern branch, similar to the other members of this clade: *P. cynocephalus* south, *P. ursinus*, and *P. ursinus griseipes*. The smaller baboons, *P. kindae* and *P. cynocephalus* DRC, are grouped together in a branch outside of the northern and southern variation. When Ward's method is applied (Figure 11b), larger distances between the northern and southern branches emerge and, possibly as a consequence, *P. kindae* and *P. cynocephalus* DRC cluster with the northern branch. For females, the first UPGMA tree (Figure 12a) does not reproduce the dichotomy between the southern and northern baboons.

However, when Ward's method is applied (Figure 12b), the dichotomy reappears, and locates *P. cynocephalus* south similar to the north and south branches (Figure 12b).

To control for the effect of potential errors due to scanning for the data we collected from the new Gorongosa specimens included here, we computed comparative trees by excluding the principal component that summarized most of the differences between the Gorongosa consensus and all the other mean population configurations (PC3). For females, this procedure works well: we observe an equidistant separation between Gorongosa and the rest of the between-group female averages (Figure 10f; PC3 = 14.4%). However, the separation is not equidistant for male mean groups (PC3 = 9.6%; Figure 10b). Thus, we place more confidence in the female phenograms after performing this correction (Figures 12c and 12d). The results for males and females mostly replicated the general topology of the previous trees, with a few exceptions. For the male phenograms (Figures 11c and 11d), Gorongosa clusters closer to *P. ursinus griseipes* and *P. ursinus* than *P. cynocephalus* south; however, the relative position of *P. papio* and *P. hamadryas* is inverted in the northern branch. For the female UPGMA tree (Figure 12c), *P. cynocephalus* south and Gorongosa cluster together; however, *P. ursinus* clusters with the northern branch. On the other hand, the female phenogram tree resulting from Ward's method (Figure 12d) supports the association of *P. cynocephalus* south and Gorongosa, and places *P. ursinus* in the southern branch.

### 3.6 Genetic and phenetic Mantel correlograms

To provide evidence that our morphometric data reflect population history, we assess the geographic pattern of morphological autocorrelation compared to an empirical model of genetic autocorrelation. To this end, we computed Mantel correlograms for the Procrustes shape coordinates, centroid size, and "size-corrected" shape residuals bounded within non-overlapping intervals of geographic distances. Only the "size-corrected" shape coordinates yielded a

statistically significant "overall" Mantel correlation ( $r_M=0.121$ ;  $P$  value=0.001; Table 9), and also for males ( $r_M=0.161$ ;  $P$  value=0.001; Table 10) and females ( $r_M=0.152$ ;  $P$  value=0.021; Table 11). We compared the "size-corrected" shape autocorrelation to genetic autocorrelation calculated from genetic distances bounded within non-overlapping intervals of geographic distances. Pairwise genetic distances were computed from publicly available mitochondrial cytochrome b (CYT-B) gene sequences ( $n=153$ ) from Zinner et al. (2009) and Keller et al. (2010). The genetic correlograms produced a statistically significant "overall" Mantel correlation ( $r_M=0.411$ ;  $P$  value=0.001; Table 12).

Figure 13 shows the CYT-B gene Mantel correlogram (Figure 13a) and the "size-corrected" shape correlograms (13b-d). The genetic and shape correlogram plots display a shared pattern of genetic similarity decay with respect to geographic distance. The CYT-B gene Mantel correlogram shows a pronouncedly steep pattern, starting with moderate positive correlation in the first distance class (class 1: 0 to 1,109 km;  $r_M=0.338$ ;  $p$ -value=0.001; Table 12) and declining towards significantly negative correlations. The "size-corrected" shape correlogram shows low positive correlation in the first distance class (class 1: 0 to 1,153 km;  $r_M=0.132$ ;  $P$  value=0.001; Table 9) and a small decrease towards negative correlations, with a flat pattern from 2,306 km (classes 3 to 6) and no statistical significance after 3,459 km (classes 4 to 6). In short, both the genetics and the morphology correlate positively at shorter geographic distances, but the correlation decreases as geographic distance increases, as expected under an isolation-by-distance model.

#### 4. Discussion

In this work, we set out to provide the first morphological assessment of the baboons in GNP, a population located close to a predicted contact area between *P. cynocephalus* and *P. ursinus*. We describe their external phenotype based on fourteen traits and features observed in

both *P. ursinus griseipes* and *P. cynocephalus*. Then, we implemented geometric morphometric techniques to place the GNP baboons within *Papio* diversity. Our results show their morphology is intermediate between *P. ursinus griseipes* and *P. cynocephalus* south.

As described by previous research, baboon craniofacial shape variation is highly related to size (Leigh and Cheverud, 1991; Collard and O'Higgins, 2002; Singleton, 2002; Frost et al., 2003; Leigh, 2006; Singleton et al., 2017) and geographic origin (Frost et al., 2003; Dunn et al., 2013). In our study, we found that allometry explains more than 30% of shape variation, which is closer to the 35% described by Frost et al. (2003). After removing the effects of size, craniofacial shape allowed us to place the baboons from Gorongosa in close relation to *P. ursinus griseipes* and *P. cynocephalus* south (Figures 11 and 12), which is expected in light of their geographic location. The "size-corrected" shape PCA averaged by groups and agglomerative-hierarchical cluster analysis reproduced the well-established subdivision of the genus *Papio* in the north and south clades (Jolly, 2003; Frost et al., 2003; Zinner et al., 2009). Within the northern clade, cluster analysis (Figures 11a-b and 12d) was concordant with the topology of mtDNA-based phylogenetic trees showing eastern olive baboons and northern yellow baboons as forming a single clade, with hamadryas being closer to this clade than Guinea baboons (see McGoogan et al., 2007). The Kinda clade is less stable and is closely related to *P. cynocephalus* DRC specimens, which could indicate that the latter are probably Kinda baboons labeled as yellow baboons before they were recognized as an independent taxon. MtDNA molecular data have placed Kinda baboons within the southern branch. However, our results suggest that, at least with respect to "size-corrected" shape, the Kinda tends to separate from the rest as a third independent clade. This finding is in agreement with results from Singleton et al. (2017) showing that the Kinda baboon differs from other species in the size, shape, and size-independent shape dimorphism patterns. The fact that Kinda falls within the northern clade when applying Ward's method (Figures 11b and 11d) could be indicative



of some sort of affinity with the northern clade. More complex demographic scenarios involving admixture between members of the northern and southern clade in generating the morphological peculiarity of the Kinda baboons might also be possible.

One unique aspect of our analysis as compared to previous morphometrics studies (see Frost et al., 2003; Dunn et al., 2013; Singleton et al., 2017) was that we took into account the *P. cynocephalus* paraphyly and treated the north and south yellow baboons separately. Zinner et al. (2009) showed that north and south yellow baboons fall into different mtDNA clades.

Furthermore, Zinner et al. (2015) delineated a division between north and south yellow baboon mtDNA clades along the Ugalla-Malagarasi River and Ruaha-Rufiji River in central Tanzania. Our results based on this approach fit the published molecular data well. More generally, they match up with the idea of a separation between southern and northern yellow baboons. Moreover, the clustering of male GNP baboons with male chacma (Figures 11c and 11d), and female GNP baboons with female southern yellow (Figures 12c and 12d) allow us to put forward, at least from skull morphology, an affinity of the GNP baboons with both, the southern yellow and chacma baboons. In addition, DFA was unable to differentiate between grayfooted chacma males and southern yellow males (Tables 4, 6 and 8), which all together, suggest that the GNP baboon phenotype fits within a geographic clinal pattern of replacing allotaxa. In conclusion, our results, showing the GNP baboon as intermediate between the yellow and the chacma, support the hypothesis of either past and/or ongoing hybridization between the grayfooted chacma and southern yellow baboons in GNP or an isolation-by-distance scenario with GNP baboons geographically and morphologically intermediate between the chacma and southern yellow baboons. The two scenarios are not mutually exclusive, as gene flow between neighboring groups could have also happened after the initial dispersal. The affinity of the female GNP baboons and

female southern yellow, and the affinity of the male GNP baboons and male chacma, could be an indication of recent hybridization.

As Jolly (1993) pointed out, some confusion existed in the past as to whether baboons from northern Mozambique, Malawi, and northwestern Zambia belong to *P. ursinus* or *P. cynocephalus*. Earlier authors interpreted this as evidence of admixture between the chacma and the yellow (Napier, 1981) or as evidence of a chacma/yellow cline (Freedman, 1963; Booth and Freedman, 1970). Currently, there is agreement that the Luangwa baboons from southwestern Zambia and Malawi are considered to be *P. cynocephalus jubilaeus* (Burrell, 2009; Zinner et al., 2015). Some authors have described finding *P. cynocephalus strepitus* in Malawi, and north-central Mozambique (Hill, 1970), including the southern margin of the Zambezi River in Catapu Reserve (Zinner et al., 2015), located 120 km north to GNP. In fact, baboons from Catapu exhibit yellow features (yellow fur, white ventral hair, circum-orbital pink skin, silvery fringe on hands and feet). However, the Mozambican Lower Zambezi is a wide river, which baboons are unlikely to cross. On the other hand, we could not discard a scenario where ancient changes in the drainage system of the Lower Zambezi River (Cotterill, 2003, 2006; McCartney and Owen, 2007; Rocha, 2014) led to secondary contact between yellow and grayfooted chacma baboons. If this were the case, GNP would be an area of hybridization.

Several phenotypic and mtDNA features link the GNP baboons to both the *P. cynocephalus* south and *P. ursinus griseipes*. This phenostructure pattern would be expected under an ongoing process of nuclear swamping and/or past admixture, rather than lineage sorting. The genetic mtDNA data available for *Papio* include two samples collected from GNP (Zinner et al., 2009). The GNP baboon mtDNA falls within haplogroup B, which is shared by the southern yellow and northern chacma baboons (as mentioned, the distribution of the northern chacma subclade most likely coincides with the subspecies *P. u. griseipes*). South yellow and grayfooted chacma mtDNA

form their own subclades within haplogroup B, while the mtDNA data from Gorongosa fall near the grayfooted chacma in the northern subclade of haplogroup B (preliminary data from an ongoing study of a larger set of samples agree with these observations). More genetic data, also analyzing the variation at the nuclear level, are necessary to fully investigate the relationships between the GNP, southern yellow, and northern chacma baboons, and to explore the underlying evolutionary dynamics (like primary or secondary hybridization).

Interestingly, Keller et al. (2010) found the same mtDNA haplotype from Gorongosa in Moremi National Park (Okavango Delta, Botswana), more than 1,200 km away from Gorongosa (haplotype NC7; Keller et al., 2010). Keller et al. (2010) also found this haplotype in Rhodes Inyanga National Park (Zimbabwe) and Alldays (R. of South Africa). The latter is located 670 km southwest of Gorongosa and 740 km southeast of Moremi, drawing a triangular area of 238.646 km<sup>2</sup>. Zinner et al. (2009) found mtDNA haplotypes belonging to the same clade more than 1,100 km apart in Namibia and South Africa. These findings are compatible with ancient shared haplotypes and/or a significant amount of past, recent, or ongoing gene flow across the grayfooted chacma baboon populations (see Sithaldeen et al., 2009, 2015) and are consistent with our Mantel correlation results. This level of gene flow may not be unexpected for baboons, given their behavioral flexibility and ability to use different habitats. Habitat modeling in West Africa by Vale et al. (2015) suggests that river valleys could work as corridors for baboons. In the more dry landscape of southern Africa, river valleys may have an even larger function as corridors. Gorongosa and Moremi are connected through the Zambezi River Valley, which is thought to have a major impact on the biogeographic structure and evolution of southern African mammal species (Cotterill, 2003; Pedersen et al., 2018). Thus, one possible explanation underlying the shared haplotypes between Moremi and Gorongosa, is that the Zambezi River Valley functions as a corridor, thus connecting distant populations of grayfooted baboons.

The results from the Mantel correlations show a positive relationship for genetic diversity at shorter geographic distances (within 1,100 km). The relationship decreases as geographic distance increases, as would be expected under an isolation-by-distance model. This result agrees with previous research suggesting isolation-by-distance using a Mantel correlation between genetic and geographic distance for different baboon species (Kopp et al., 2014, 2015). In our study, only after removing the effects of size does morphology correlate with the above-mentioned genetic pattern. The lack of correlation when looking at craniofacial morphology at longer distances might be due to drift or local pressures, which make it deviate from simple linearity. It is likely that at longer distances, many of the comparisons end up being across different ecological zones. The match between genetic and morphological correlation to geographic distance validates the use of the "size-corrected" craniofacial shape in our comparative morphometric analysis and confirms that craniofacial complexity still retains population history signals (Cardini and Elton, 2008).

Finally, these results provide new evidence and a novel framework to interpret the evolutionary processes influencing the diversity, distribution, and structure of *Papio* species. More broadly, papionin species have long been considered a useful model to understand processes occurring in early human evolution (Jolly, 2001). The data provided here might be useful in the interpretation of hominin fossils separated by distances similar to those of *Papio* populations (in some cases, >1000 km). For example, Middle Pleistocene hominins from sites such as Bodo (Ethiopia), Kabwe (Zambia), and Elandsfontein (South Africa), may be considered representative of different species or populations of a species, depending on the framework for comparison (Rightmire, 2013). The baboon data provide a useful empirical framework for considering variation and possible gene flow across widely separated early hominin populations (or species).

665

666 **Acknowledgements**

667 The Gorongosa Paleo-Primate Project would like to thank the Gorongosa Restoration Project, the  
668 National Geographic Society (Grant Number GEFNE169-16), the John Fell Fund, and the Philip  
669 Leverhulme Prize (PLP-2016-114) awarded to S. Carvalho, for their generous support with starting  
670 this interdisciplinary endeavor. Our work is only possible due to the visionary approach of Greg  
671 Carr and the dedicated staff from Gorongosa National Park, guided by Dr. Mateus Mutemba. We  
672 are very grateful to Dr. Solange Macamo, Dr. Mussa Raja at Universidade Eduardo Mondlane, and  
673 to all the Park "fiscais," and to our students and colleagues from across many institutions who  
674 have been very enthusiastic about this project. F. I. Matinez is funded by *Vicerrectoría de*  
675 *Investigación, Pontificia Universidad Católica de Chile, Concurso Estadías y Pasantías Breves 2016.*  
676 C. Capelli is grateful for support from St. Hugh's College, University of Oxford. M. Ferreira da Silva  
677 is currently a Foundation for Science and Technology postdoctoral fellow (SFRH/BPD/88496/2012).  
678 We would also like to thank Sarah Elton for sharing the database from Dunn et al. (2013); Carolyn  
679 McCallister for her help in revising the manuscript; Michael Haworth, Daniel Cara, Megan  
680 Petersdorf, Jim Auburn, John Weir, Thomas M. Butynski and Yvonne A. de Jong for granting  
681 permission to use their photographs of baboons. We further thank Clifford Jolly for his invaluable  
682 feedback and comments on Gorongosa baboon morphological features.

683 **Author contributions:**

684 S.C. and R.B. conceived and co-direct the PPP project. F.I.M., C.C. and M.F.d.S. conceived the  
685 morphometric and genetics study. F.I.M. analyzed the data and wrote the manuscript. C.C.,  
686 M.F.d.S., R.B. and S.C. contributed to manuscript writing. V.A., Z.A., W.A., M.B., D.B., D.R.B., E.C.,  
687 J.H., T.L., H.M., J.M., L.M.P., M.P., M.S. and F.T. contributed to field work and edited the  
688 manuscript. All authors read and approved the final version of the manuscript.

689

690 **References**

- 691 Altmann, J., Altmann, S., Hausfater, G., 1981. Physical maturation and age estimates of yellow  
692 baboons, *Papio cynocephalus*, in Amboseli National Park, Kenya. American Journal of Primatology  
693 1, 1389–399.
- 694 Alberts, S., Altmann, J., 2001. Immigration and hybridization patterns of yellow and anubis  
695 baboons in and around Amboseli, Kenya. American Journal of Primatology 53, 139–154.
- 696 Barrett, L., Henzi, S. P., 2008. Baboons. Current Biology 18, R404–R406.
- 697 Bookstein, F.L., 1991. Morphometric tools for landmark data: Geometry and biology. Cambridge:  
698 Cambridge University Press.
- 699 Booth, S., Freedman, L., 1970. Multivariate discriminant analysis applied to cranial features of *P.*  
700 *ursinus* and *P. cynocephalus*. Folia Primatologica 12, 276–289.
- 701 Borcard, D., Legendre, P., 2012. Is the Mantel correlogram powerful enough to be useful in  
702 ecological analysis? A simulation study. Ecology 93, 1473–1481.
- 703 Burrell, A., 2009. Phylogenetics and population genetics of Central African baboons. PhD thesis.  
704 New York University, Department of Anthropology.
- 705 Cardini, A., Elton, S., 2008. Does the skull carry a phylogenetic signal? Evolution and modularity in  
706 the guenons. Biological Journal of the Linnean Society 93, 813–834.
- 707 Cardini, A., Jansson, A.-U., Elton, S., 2007. A geometric morphometric approach to the study of  
708 ecogeographical and clinal variation in vervet monkeys. Journal of Biogeography 34, 1663–1678.
- 709 Chiou, K.L., 2018. <http://kennychiou.com/dissertation/>. Last accessed: 28 February 2018.
- 710 Copes, L. E., Lucas, L. M., Thostenson, J.O., Hoekstra, H.E., Boyer, D.M., 2016. A collection of non-  
711 human primate computed tomography scans housed in MorphoSource, a repository for 3D data.  
712 Science Data 3, 160001.

713 Collard, M., O'Higgins, P., 2001. Ontogeny and homoplasy in the papionin monkey face. *Evolution*  
714 *and Development* 3, 322–331.

715 Cotterill, F.P.D., 2003. Geomorphological influences on vicariant evolution in some African  
716 mammals in the Zambezi Basin: some lessons for conservation. In: Plowman, A. (ed.), *Ecology and*  
717 *Conservation of Mini-antelope: Proceedings of an International Symposium on Duiker and Dwarf*  
718 *Antelope in Africa*. Fürth / Germany: Filander Verlag, pp 11–58.

719 Cotterill, F.P.D., 2006. The evolutionary history and taxonomy of the *Kobus leche* species complex  
720 of South- Central Africa in the context of palaeo-drainage dynamics. Stellenbosch: Stellenbosch  
721 University.

722 Cracraft, J., 1983. Species concepts and speciation analysis. In: Johnston, R.F. (Ed.) *Current*  
723 *Ornithology*. Plenum Press, New York, pp 159–187.

724 Diniz-Filho, J.A.F., Soares, T.N., Lima, J.S., Dobrovolski, R., Landeiro, V.L., de Campos Telles, M.P.,  
725 Rangel, T.F., Bini, L.M., 2013. Mantel test in population genetics. *Genetics and Molecular Biology*  
726 36, 475–485.

727 Dobzhansky, T., 1937. *Genetics and the origin of species*. Columbia University Press, New York.

728 Drake, A.G., Klingenberg, C.P., 2008. The pace of morphological change: historical transformation  
729 of skull shape in St Bernard dogs. *Proceedings of The Royal Society B* 275, 71–76.

730 Dray, S., Dufour, A.B., 2007. The ade4 package: implementing the duality diagram for ecologists.  
731 *Journal of Statistical Software* 22, 1–20.

732 Dunbar, R.I.M., 1990. Environmental determinants of intraspecific variation in body weight in  
733 baboons (*Papio spp.*). *Journal of Zoology* 220, 157–169.

734 Dunn, J., Cardini, A., Elton, S., 2013. Biogeographic variation in the baboon: dissecting the cline.  
735 *Journal of Anatomy* 223, 337–352.

736 Fischer, J., Kopp, G.H., Dal Pesco, F., Goffe, A., Hammerschmidt, K., Kalbitzer, U., Klapproth, M.,  
 737 Maciej, P., Ndao, I., Patzelt, A., Zinner, D., 2017. Charting the neglected West: The social system of  
 738 Guinea baboons. *American Journal of Physical Anthropology* 162, 15–31.  
 739 Freedman, L., 1963. A biometric study of *Papio cynocephalus* skulls from Northern Rhodesia and  
 740 Nyasaland. *Journal of Mammalogy* 44, 24–43.  
 741 Frost, S.R., Marcus, L.F., Bookstein, F.L., Reddy, D.P., Delson, E., 2003. Cranial allometry,  
 742 phylogeography, and systematics of large-bodied papionins (primates: Cercopithecinae) inferred  
 743 from geometric morphometric analysis of landmark data. *The Anatomical Record Part A:*  
 744 *Discoveries in Molecular, Cellular, and Evolutionary Biology* 275, 1048–1072.  
 745 Grubb, P., 1999. Evolutionary processes implicit in distribution patterns of modern African  
 746 mammals. In: Bromage, T.G., Schrenk, F. (Eds.), *African biogeography, climate change and human*  
 747 *evolution*. New York: Oxford University Press, pp. 150–164.  
 748 Guillot, G., Rousset, F., 2013. Dismantling the Mantel tests. *Methods in Ecology and Evolution* 4,  
 749 336–344.  
 750 Hammer, Ø., Harper, D.A.T., 2008. *Paleontological Data Analysis*. Blackwell, Oxford.  
 751 Hill, W.C.O., 1970. *Primates: Comparative anatomy and taxonomy*. Vol. 8. Cynopithecinae: *Papio*,  
 752 *Mandrillus*, *Theropithecus*. Edinburgh University Press, Edinburgh, Scotland.  
 753 Hoffmann, M., Hilton-Taylor, C., 2008. *Papio ursinus* (errata version published in 2016). The IUCN  
 754 Red List of Threatened Species 2008: e.T16022A99710253.  
 755 <http://dx.doi.org/10.2305/IUCN.UK.2008.RLTS.T16022A5356469.en>. Downloaded on 30 October  
 756 2017.  
 757 IUCN (International Union for Conservation of Nature) 2008. The IUCN Red List of Threatened  
 758 Species. Version 2017-3. <[www.iucnredlist.org](http://www.iucnredlist.org)>. Downloaded on 18 March 2018.



759 Jolly, C.J., 1993. Species, subspecies and baboons systematic. In: Kimbel, W.H., Martin, L.B. (Eds.),  
760 Species, Species Concepts and Primate Evolution. Springer Science, New York, pp 67–108.

761 Jolly, C.J., 2001. A proper study for Mankind: analogies from the *Papionin* monkeys and their  
762 implications for human evolution. Yearbook of Physical Anthropology 44, 177–204.

763 Jolly, C.J., 2003. Cranial anatomy and baboon diversity. The Anatomical Record Part A 275, 1043–  
764 1047.

765 Jolly, C.J., Burrell, A.S., Phillips-Conroy, J.E., Bergey, C., Rogers, J., 2011. American Journal of  
766 Primatology 73, 291–303.

767 Keller, C., Roos, C., Groeneveld, L.F., Fischer J., Zinner, D., 2010. Introgressive hybridization in  
768 Southern African baboons shapes patterns of mtDNA variation. American Journal of Physical  
769 Anthropology 142, 125–136.

770 Kingdon, J., 1997. The Kingdon field guide to African mammals. London: Academic Press.

771 Kingdon, J., Butynski, T.M., De Jong, Y., 2016. *Papio cynocephalus*. The IUCN Red List of Threatened  
772 Species 2016: e.T92250442A92250811. [http://dx.doi.org/10.2305/IUCN.UK.2016-](http://dx.doi.org/10.2305/IUCN.UK.2016-1.RLTS.T92250442A92250811.en)  
773 [1.RLTS.T92250442A92250811.en](http://dx.doi.org/10.2305/IUCN.UK.2016-1.RLTS.T92250442A92250811.en). Downloaded on 30 October 2017.

774 Klingenberg, C. P., 2011. MorphoJ: An integrated software package for geometric morphometrics.  
775 Molecular Ecology Resources 11, 353–357.

776 Klingenberg, C.P., Monteiro, L.R. 2005 Distances and directions in multidimensional shape spaces:  
777 implications for morphometric applications. Systematic Biology 54, 678–688.

778 Klingenberg, C.P., Marugán-Lobón, J., 2013. Evolutionary covariation in geometric morphometric  
779 data: analyzing integration, modularity, and allometry in a phylogenetic context. Systematic  
780 Biology 62, 591–610.

781 Kopp, G.H., Ferreira da Silva, M.J., Fischer, J., Brito, J.C., Regnaut, S., Roos, C., Zinner, D., 2014. The  
782 Influence of Social Systems on Patterns of Mitochondrial DNA Variation in Baboons. *International*  
783 *Journal of Primatology* 35, 210–225.

784 Kopp, G.H., Fischer, J., Patzelt, A., Roos, C., Zinner, D., 2015. Population genetic insights into the  
785 social organization of Guinea baboons (*Papio papio*): Evidence for female-biased dispersal.  
786 *American Journal of Primatology* 77, 878–889.

787 Le Boulengé, É., Legendre, P., de le Court, C., Le Boulengé-Nguyen, P., Languy, M., 1996.  
788 Microgeographic morphological differentiation in Muskrats. *Journal of Mammalogy* 77, 684–701.

789 Legendre, P., Fortin, M.-J., Borcard, D., 2015. Should the Mantel test be used in spatial analysis?  
790 *Methods in Ecology and Evolution* 6, 1239–1247.

791 Legendre, P., Legendre, L., 1998. Numerical ecology. Second English Edition. Elsevier Science BV,  
792 Amsterdam, The Netherlands.

793 Leigh, S.R., 2006. Cranial ontogeny of *Papio* baboons (*Papio hamadryas*). *American Journal of*  
794 *Physical Anthropology* 130, 71–84.

795 Leigh, S.R., Cheverud, J.M., 1991. Sexual dimorphism in the baboon facial skeleton. *American*  
796 *Journal of Physical Anthropology* 84, 193–208.

797 Matesanz, S., Gimeno, T.E., de la Cruz, M., Escudero, A., Valladares, F., 2011. Competition may  
798 explain the fine-scale spatial patterns and genetic structure of two co-occurring plant congeners.  
799 *Journal of Ecology* 99, 838–848.

800 Mayr, E., 1942. Systematics and the origin of species. Columbia University Press, New York.

801 Mayr, E., 1982. The growth of biological thought: diversity, evolution, and inheritance. Harvard  
802 University Press, Cambridge, MA.

803 McCartney, M., Owen, O., 2007. Technical Note: Hydrology of the Lake Urema wetland,  
804 Mozambique.

805 McGoogan, K., Kivell, T., Hutchison, M., Young, H., Blanchard, S., Keeth, M., Lehman, S.M., 2007.  
806 Phylogenetic diversity and the conservation biogeography of African primates. *Journal of*  
807 *Biogeography* 34, 1962–1974.

808 Mitteroecker, P., Bookstein, F., 2011. Linear discrimination, ordination, and the visualization of  
809 selection gradients in modern morphometrics. *Evolutionary Biology* 38, 100–114.

810 Napier, P.H., 1981. Catalogue of the Primates in the British Museum (Natural History) and  
811 Elsewhere in the British Isles. Part II: Family Cercopithecidae, Subfamily Cercopithecinae. London:  
812 British Museum (Natural History).

813 Newman, K.T., Jolly, C.J., Rogers, J., 2004. Mitochondrial phylogeny and systematics of baboons  
814 (*Papio*). *American Journal of Physical Anthropology* 124, 17–27.

815 Oksanen, J., Blanchet, F. G., Friendly, M., Kindt R., Legendre, P., McGlinn, D., Minchin, P.R., O'Hara,  
816 R. B., Simpson, G.L., Solymos, P., Stevens, M.H.H., Szoecs, E., Wagner, E., 2018). VEGAN:  
817 Community Ecology Package. R package version 2.4-6. <https://CRAN.R-project.org/package=vegan>

818 Paradis E., Claude J., Strimmer K., 2004. APE: analyses of phylogenetics and evolution in R  
819 language. *Bioinformatics* 20: 289–290.

820 Pedersen, C.-E.T., Albrechtsen, A., Etter, P.D., Johnson, E.A., Orlando, L., Chikhi, L., Siegmund,  
821 H.R., Heller, R., 2018. A southern African origin and cryptic structure in the highly mobile plains  
822 zebra. *Nature Ecology & Evolution* 2, 491–498.

823 Phillips-Conroy, J.E., Jolly, C.J., 1986. Changes in the structure of the baboon hybrid zone in the  
824 Awash National Park, Ethiopia. *American Journal of Physical Anthropology*, 71, 337–350.

825 Püschel, T.A., Gladman, J.T., Bobe, R., Sellers, W.I., 2017. The evolution of the platyrrhine talus: A  
826 comparative analysis of the phenetic affinities of the Miocene platyrrhines with their modern  
827 relatives. *Journal of Human Evolution* 111, 179–201.

828 R Core Team, 2017. R: A language and environment for statistical computing. R Foundation for  
 829 Statistical Computing, Vienna.  
 830 Rightmire, G.P., 2013. Homo erectus and Middle Pleistocene hominins: Brain size, skull form, and  
 831 species recognition. *Journal of Human Evolution* 65, 223–252.  
 832 Rocha, J.M.L., 2014. The maternal history of the sable antelope (*Hippotragus niger*) inferred from  
 833 the genomic analysis of complete mitochondrial sequences. MSc. Thesis, University of Porto.  
 834 Samuels, A., Altmann, J., 1986. *International Journal of Primatology*, 7, 131–138.  
 835 Schliep K.P., 2011. Phangorn: phylogenetic analysis in R. *Bioinformatics* 27, 592–593.  
 836 Slice, D.E., 2001. Landmark coordinates aligned by Procrustes analysis do not lie in Kendall’s shape  
 837 space. *Systematic Biology* 50:141–149.  
 838 Sholts, S.B., Flores, L., Walker, P.L., Wärmländer, S.K.T.S., 2011. Comparison of coordinate  
 839 measurement precision of different landmark types on human crania using a 3D laser scanner and  
 840 a 3D digitiser: Implications for applications of digital morphometrics. *International Journal of*  
 841 *Osteoarchaeology* 21, 535–543.  
 842 Singleton, M., 2002. Patterns of cranial shape variation in the Papionini (Primates:  
 843 Cercopithecinae). *Journal of Human Evolution* 42, 547–578.  
 844 Singleton, M., Seitelman, B.C., Krecioch, J.R., Frost, S.R., 2017. Cranial sexual dimorphism in the  
 845 Kinda baboon (*Papio hamadryas kindae*). *American Journal of Physical Anthropology* 164, 665–  
 846 678.  
 847 Sithaldeen, R., Bishop, J.M., Ackermann, R.R., 2009. Mitochondrial DNA analysis reveals Plio-  
 848 Pleistocene diversification within the chacma baboon. *Molecular Phylogenetics and Evolution* 53,  
 849 1042–1048.  
 850 Sithaldeen, R., Ackermann, R.R., Bishop, J.M., 2015. Pleistocene aridification cycles shaped the  
 851 contemporary genetic architecture of southern African baboons. *PLoS One* 10:e0123207.

852 Stalling D., Westerhoff M., Hege H.C., 2005. Amira: a highly inter-active system for visual data  
 853 analysis. In: Hansen C.D., Johnson C.R., (Eds.), The Visualization Handbook, Amsterdam, Elsevier, pp  
 854 749–767.

855 Swedell, L., 2011. African papionins: Diversity of social organization and ecological flexibility. In  
 856 Campbell, C.J., Fuentes, A., MacKinnon, K.C., Bearder, S.K., Stumpf, R.M., (Eds.), Primates in  
 857 perspective (2nd ed.). New York: Oxford University Press, pp. 241–277.

858 Tinley, K. L., 1977. Framework of the Gorongosa ecosystem Mozambique. PhD Dissertation,  
 859 University of Pretoria.

860 Vale, C.G., Ferreira da Silva, M.J., Campos, J.C., Torres, J., Brito, J.C., 2015. Applying species  
 861 distribution modelling to the conservation of an ecologically plastic species (*Papio papio*) across  
 862 biogeographic regions in West Africa. Journal for Nature Conservation 27, 26–36.

863 Vavrek, Matthew J., 2011. Fossil: palaeoecological and palaeogeographical analysis tools.  
 864 Palaeontologia Electronica 14, 1T. [http://palaeo-electronica.org/2011\\_1/238/index.html](http://palaeo-electronica.org/2011_1/238/index.html)

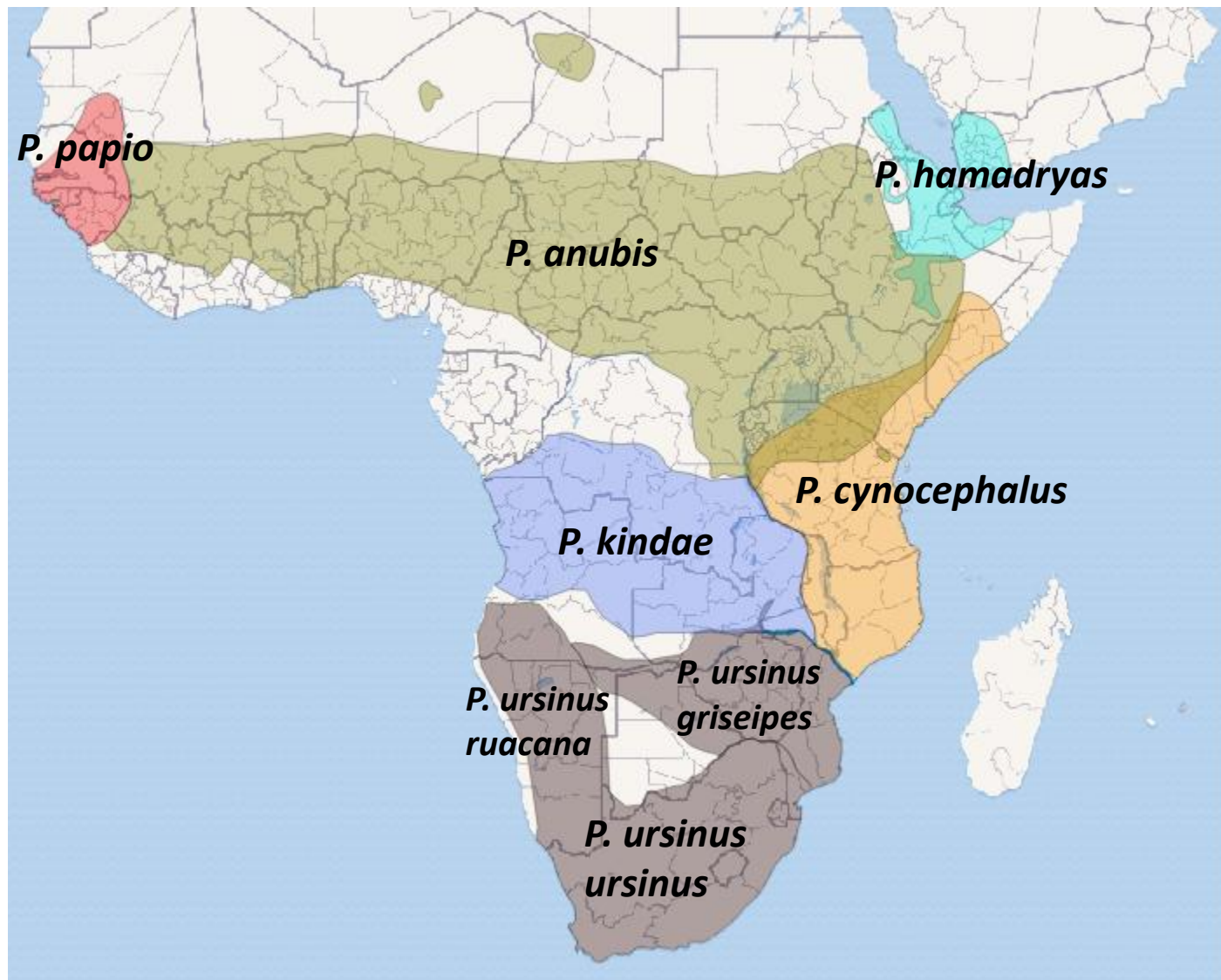
865 Zinner, D., Groeneveld, L.F., Keller, C., Roos, C., 2009. Mitochondrial phylogeography of baboons  
 866 (*Papio* spp.): indication for introgressive hybridization? BMC Evolutionary Biology 9, 83.

867 Zinner, D., Arnold, M.L., Roos, C., 2011a. The strange blood: natural hybridization in primates.  
 868 Evolutionary Anthropology 20, 96–103.

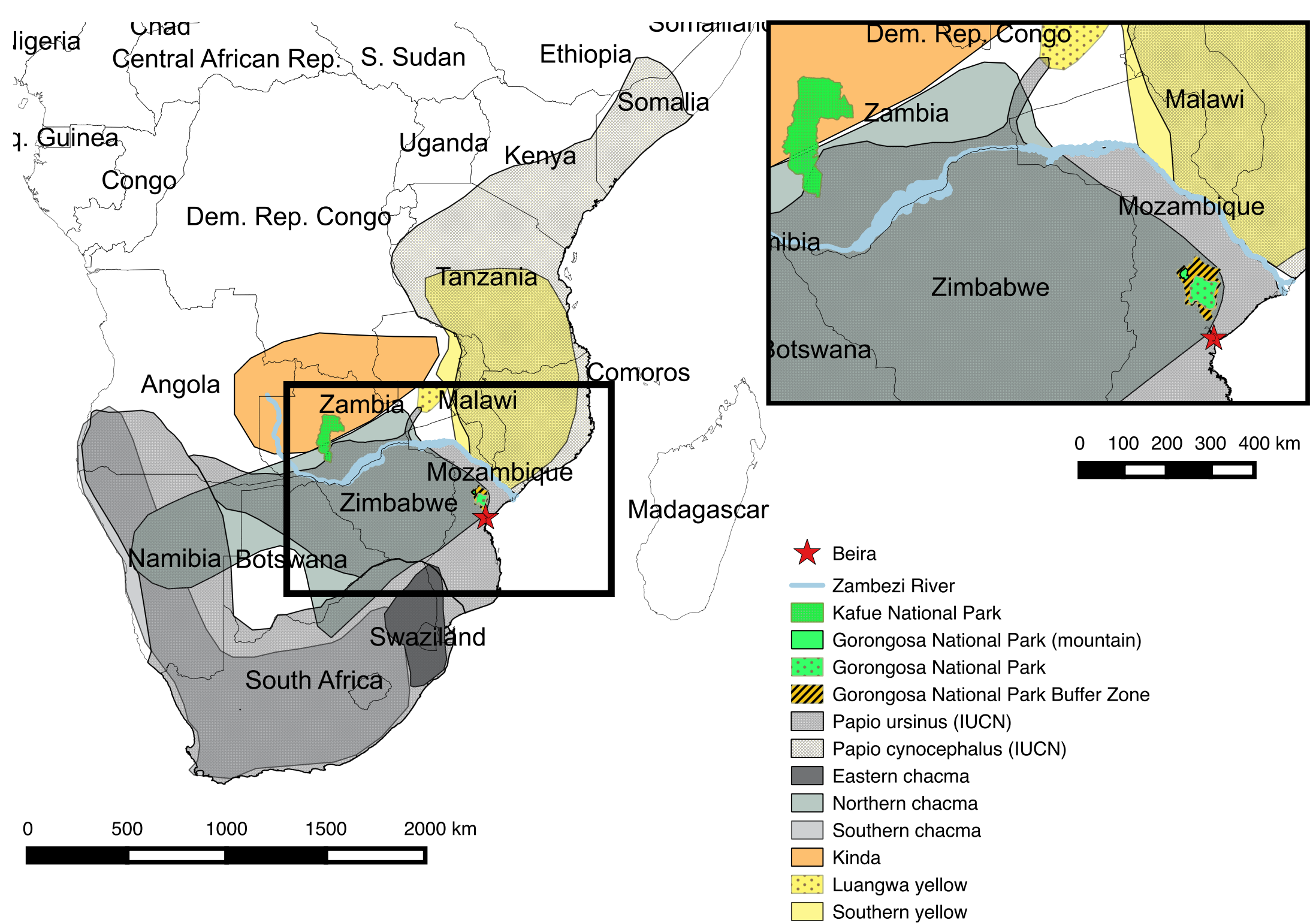
869 Zinner, D., Buba, U., Nash, S., Roos, C., 2011b. Pan-African Voyagers: The Phylogeography of  
 870 Baboons. In: Sommer, V., Ross, C. (Eds.), Primates of Gashaka: Socioecology and Conservation in  
 871 Nigeria's Biodiversity Hotspot. Springer New York, New York, NY, pp 319–358.

872 Zinner, D., Keller, C., Nyahongo, J.W., Butynski, T.M., Jong, Y.A. de, Pozzi, L., Knauf, S., Liedigk, R.,  
 873 Roos, C., 2015. Distribution of Mitochondrial Clades and Morphotypes of Baboons *Papio* spp.  
 874 (Primates: Cercopithecidae) in Eastern Africa. Journal of East African Natural History 104, 143–168.

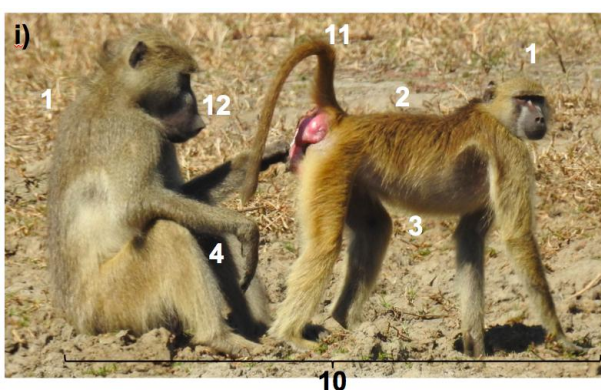
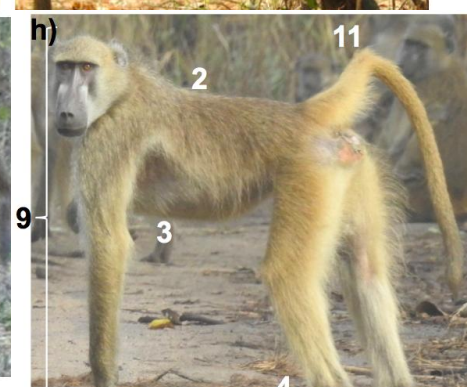
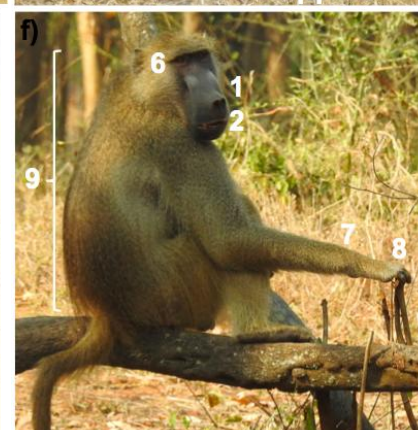
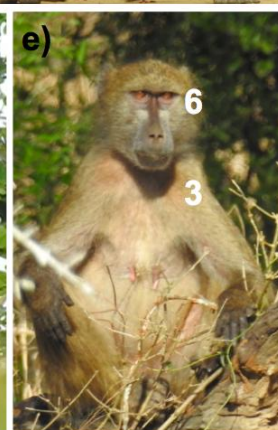
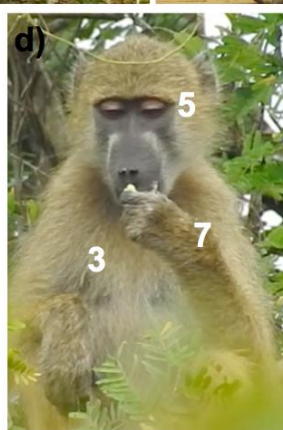
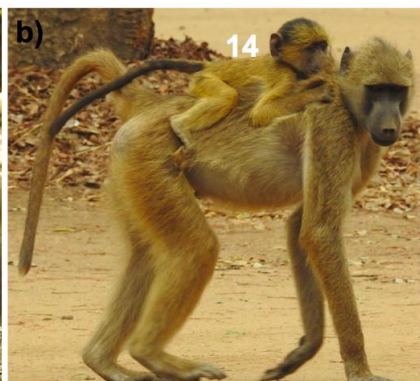
875







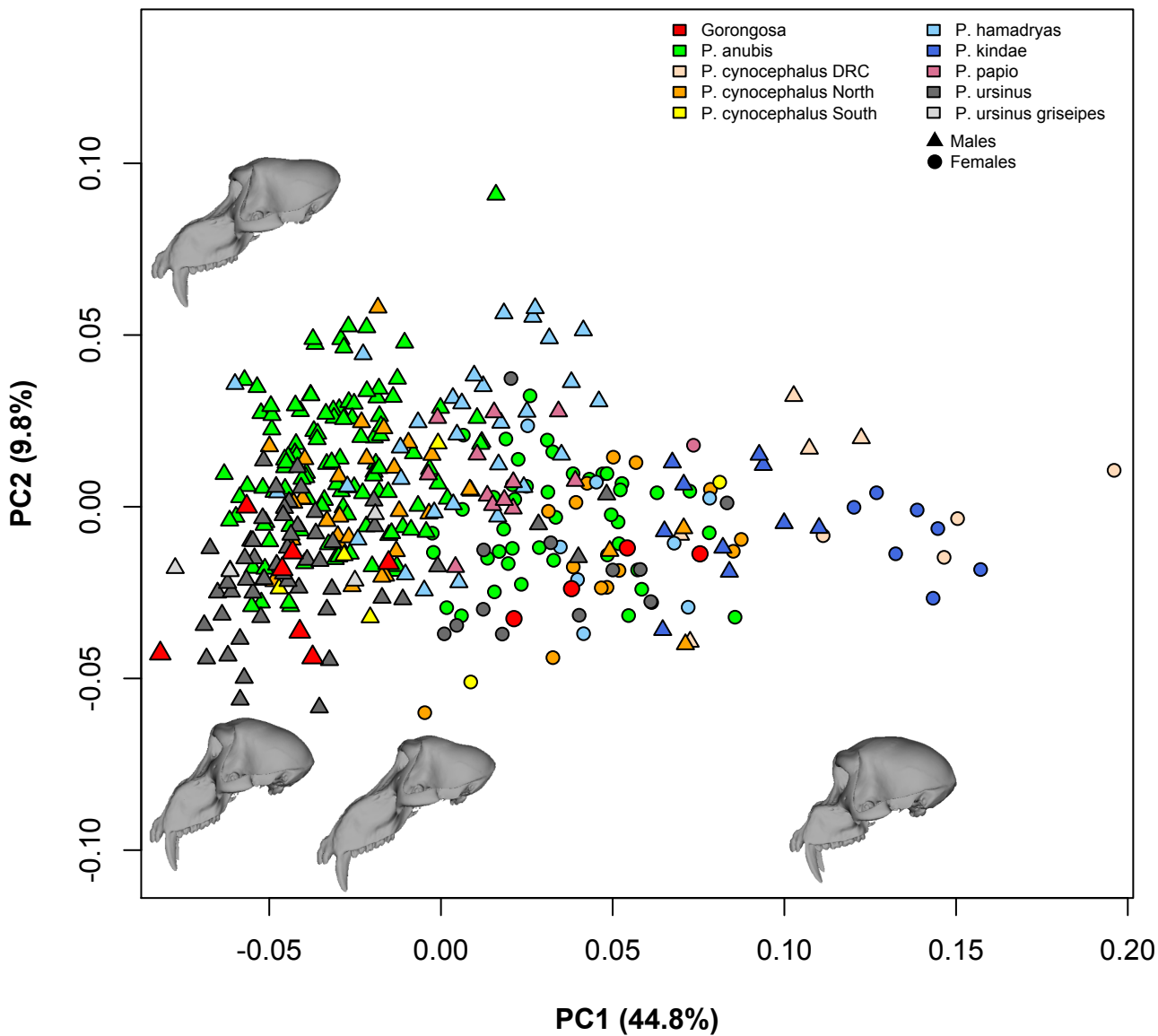


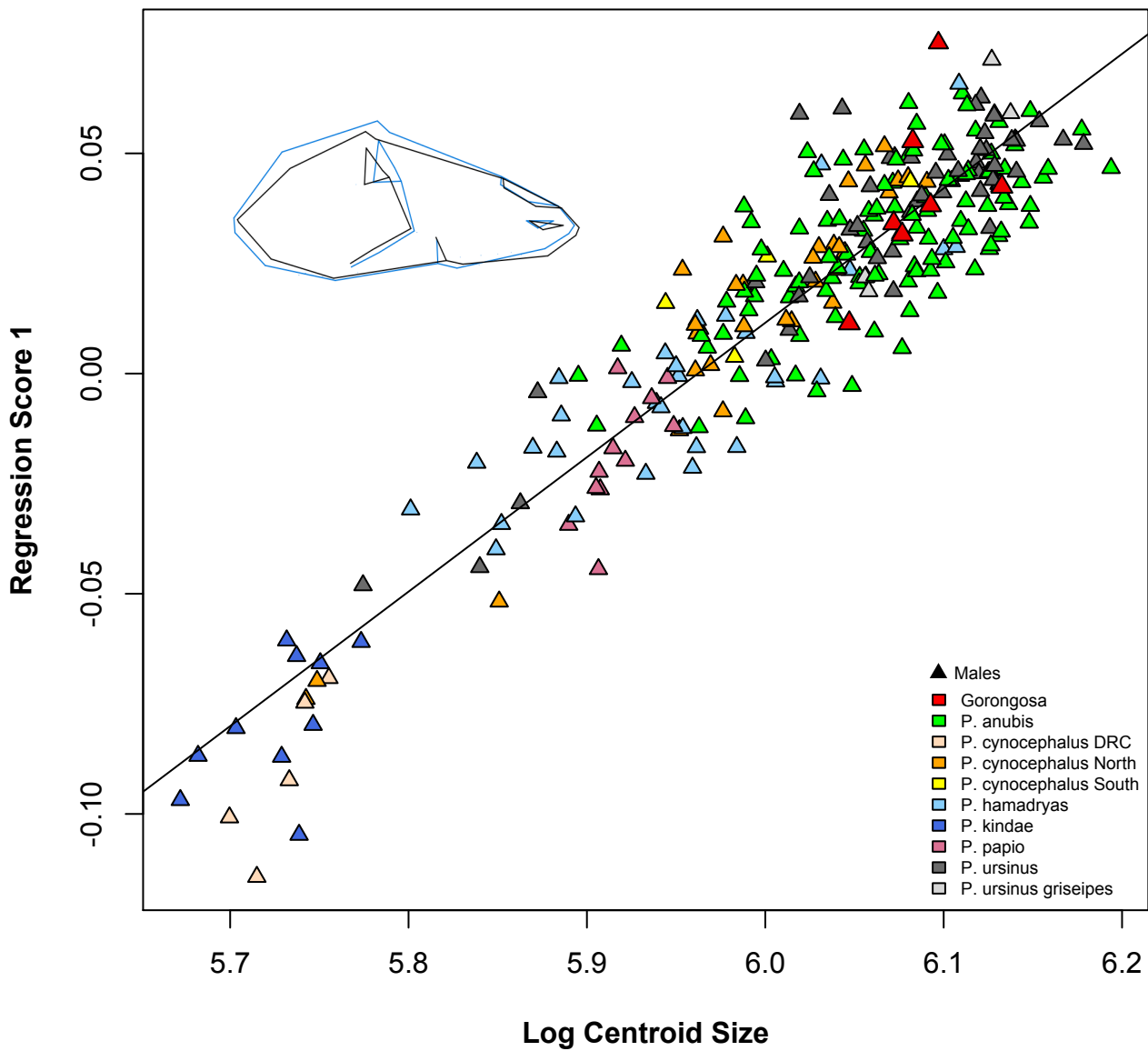


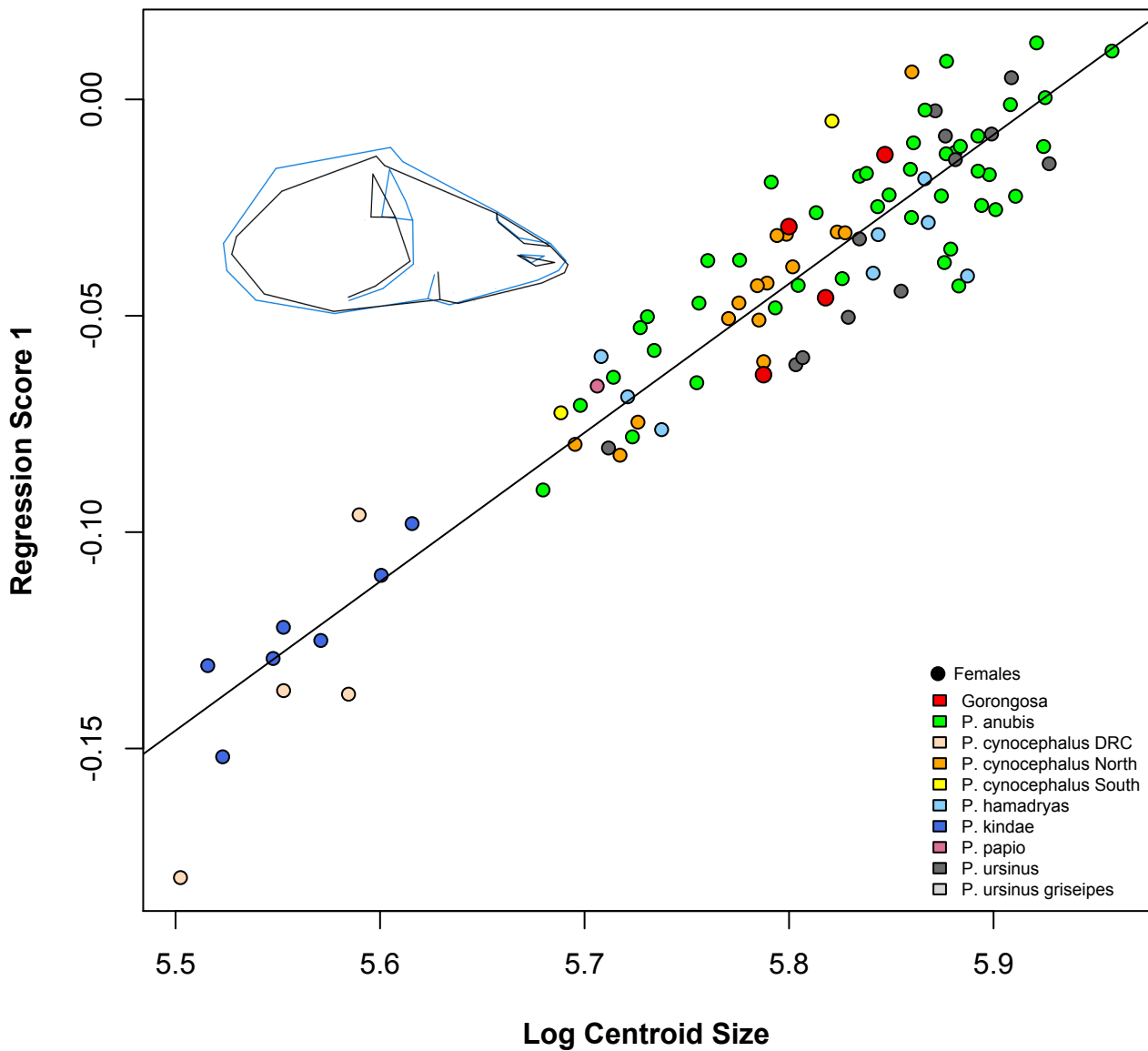


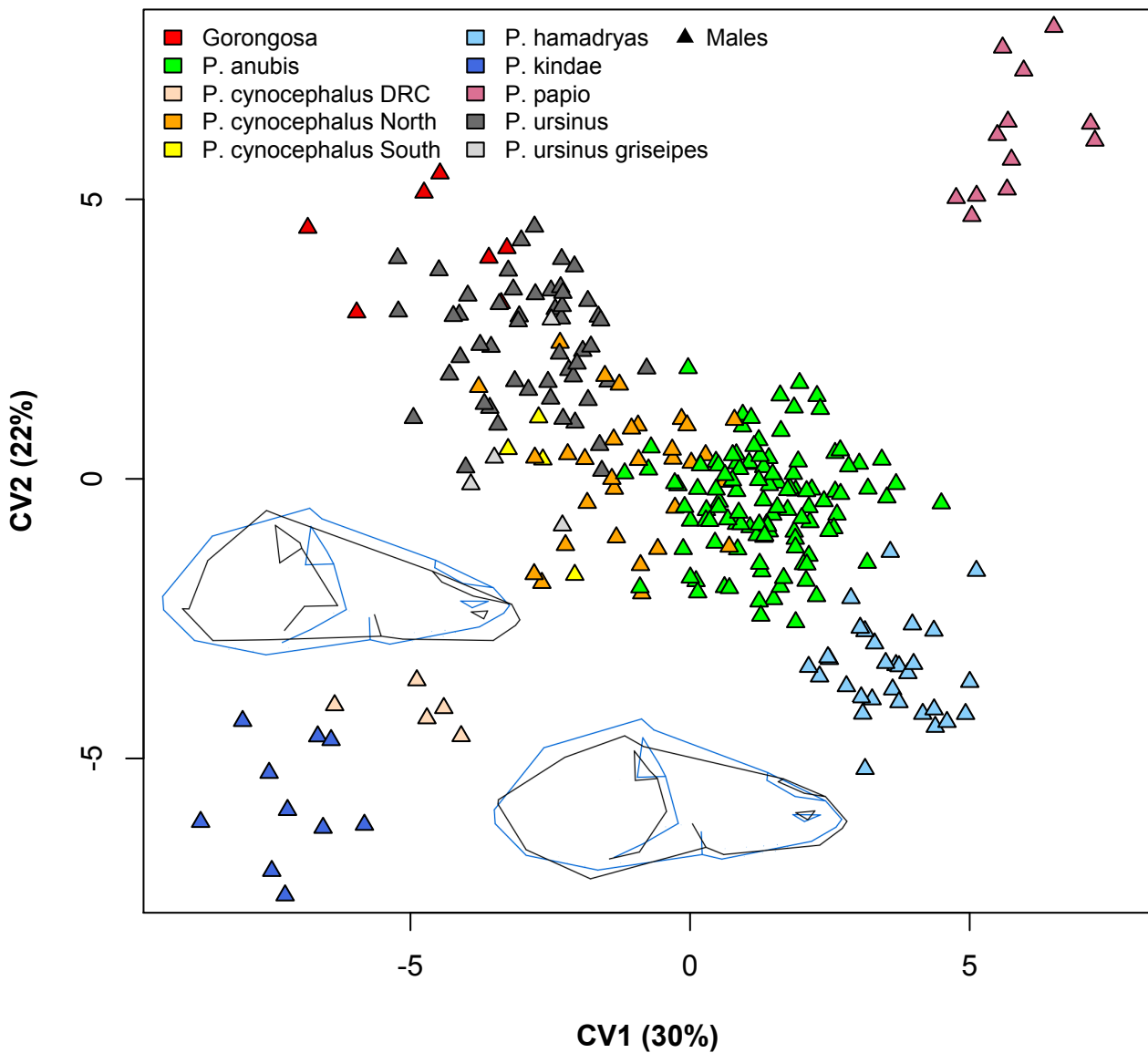




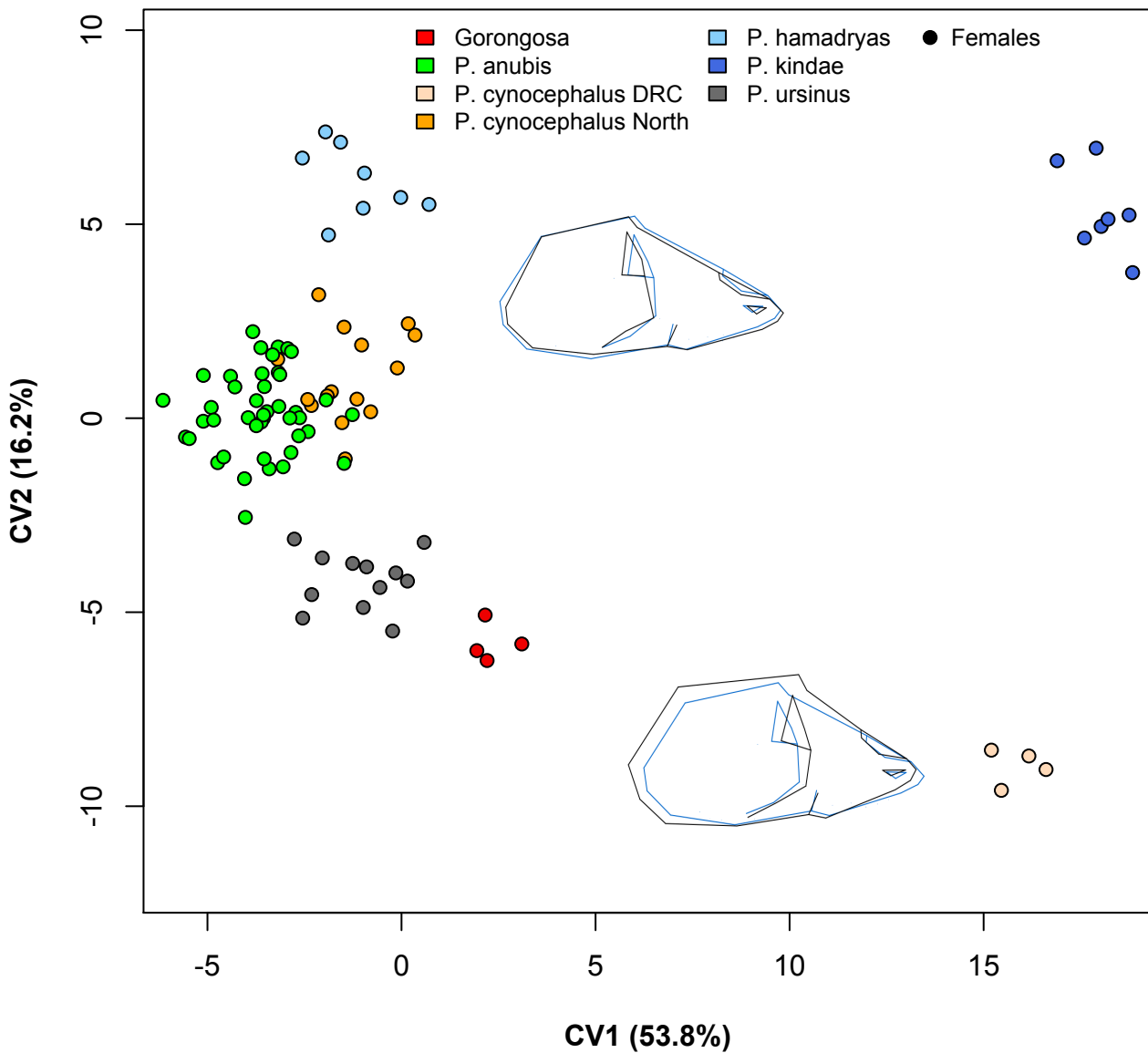


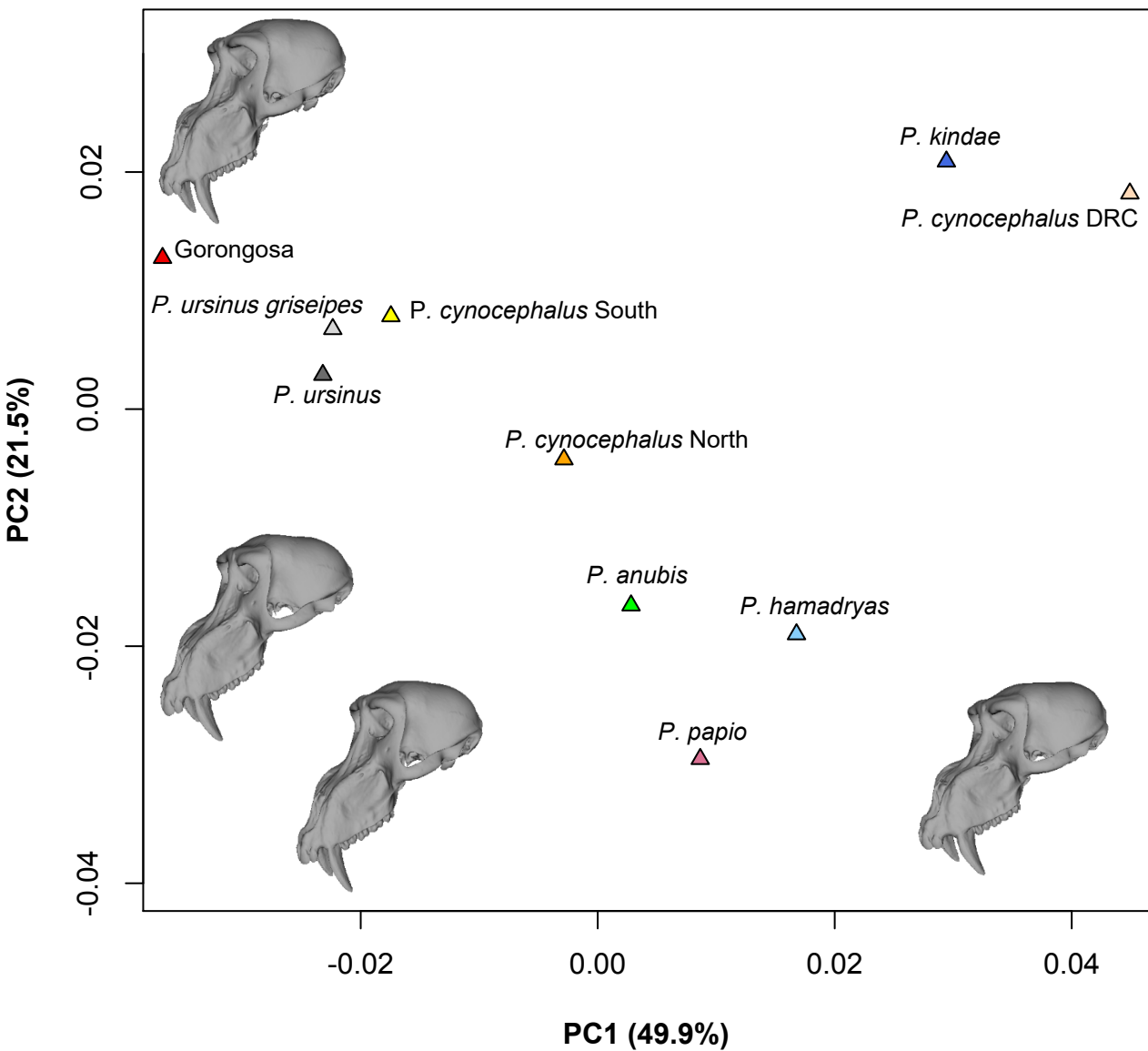




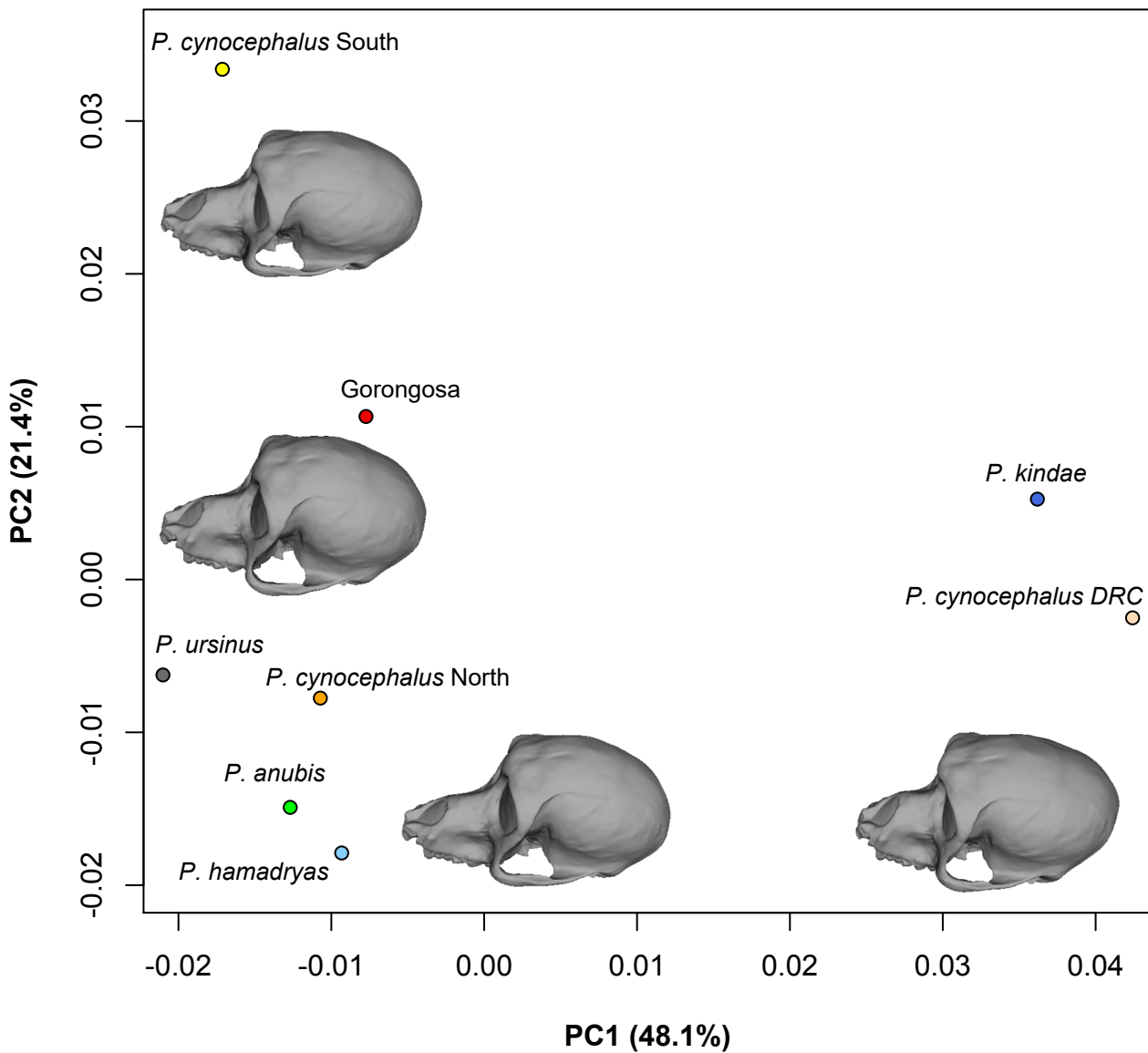


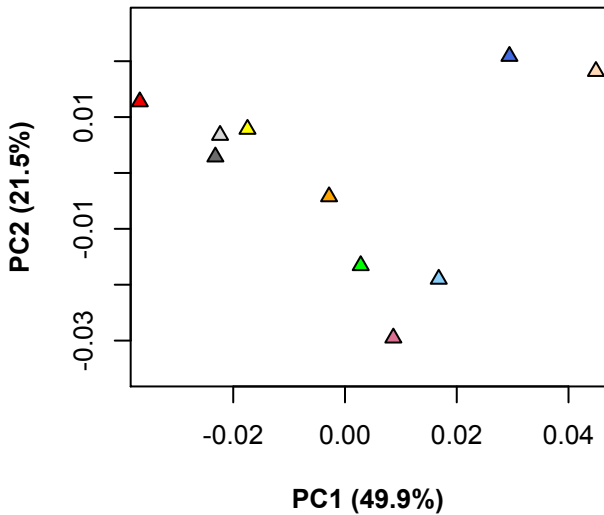
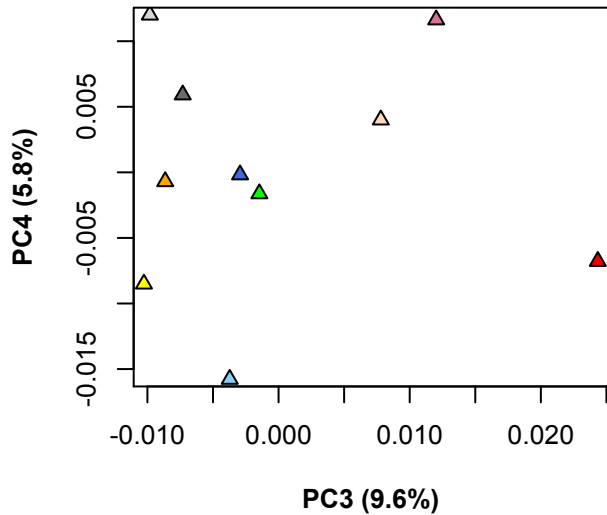
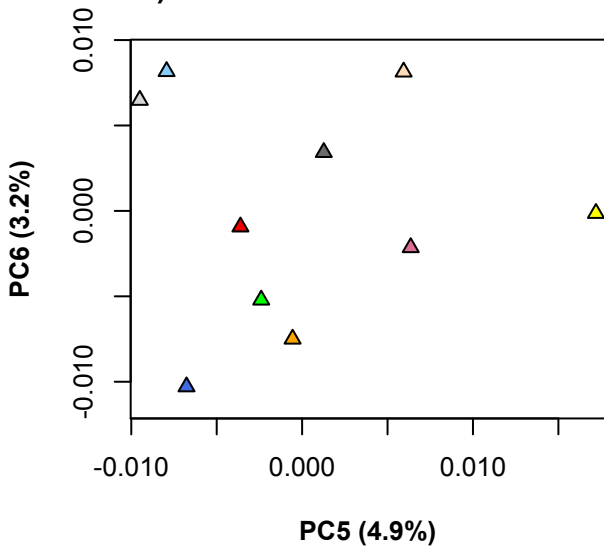
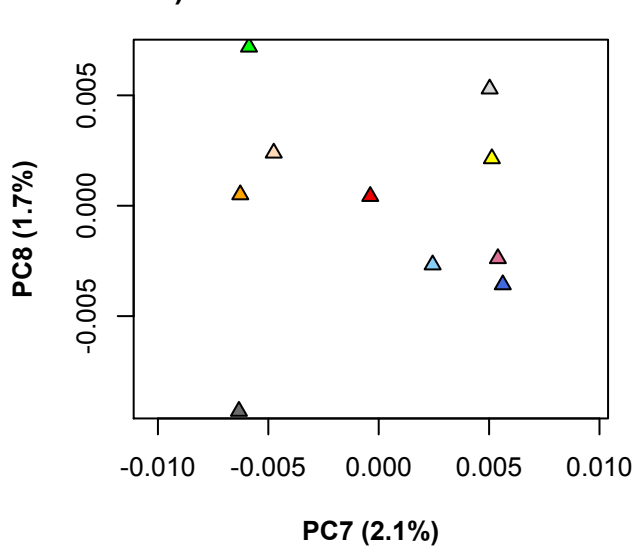


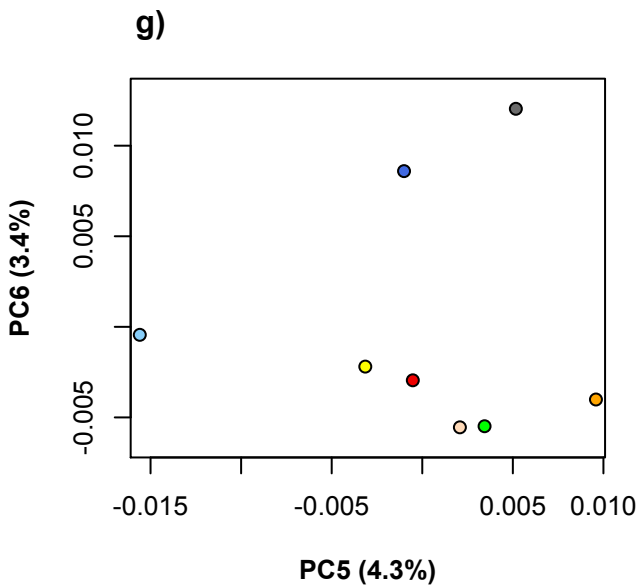
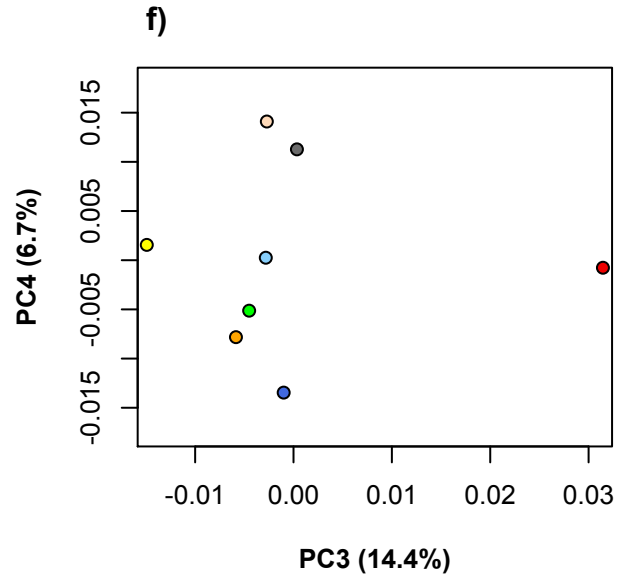
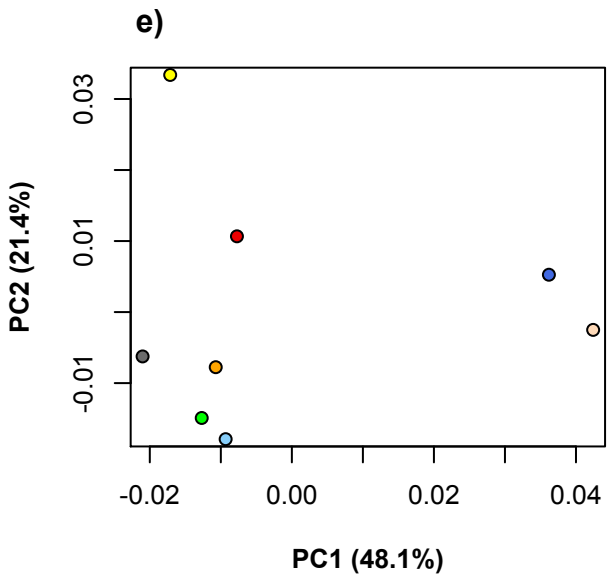








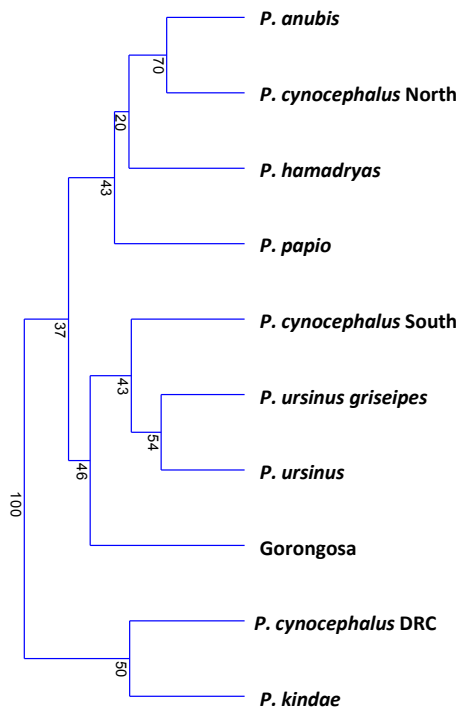
**a)****b)****c)****d)**



- Gorongosa
- P. anubis
- P. cynocephalus DRC
- P. cynocephalus North
- P. cynocephalus South
- P. hamadryas
- P. kindae
- P. papio
- P. ursinus
- P. ursinus griseipes
- ▲ Males
- Females

Euclidean distance

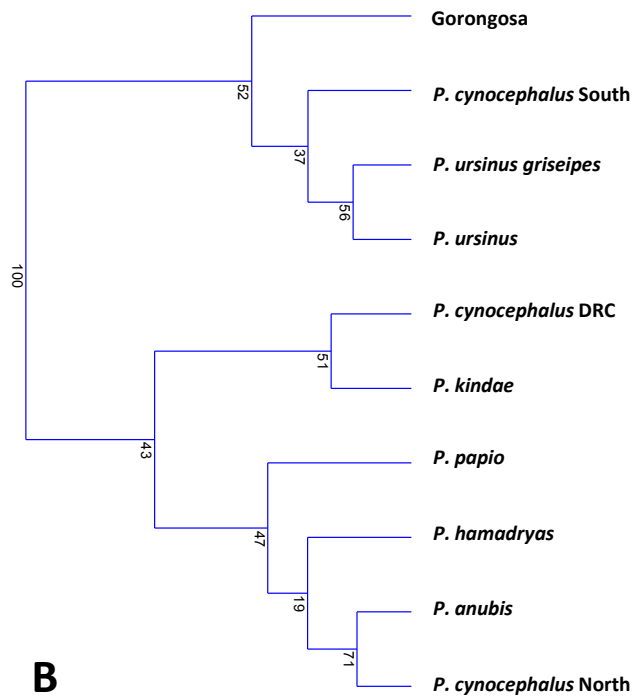
0.12 0.06 0.00



A

Euclidean distance

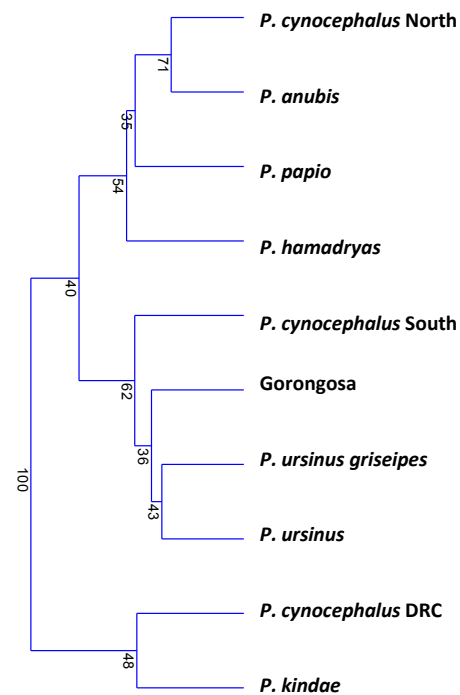
0.12 0.06 0.00



B

Euclidean distance

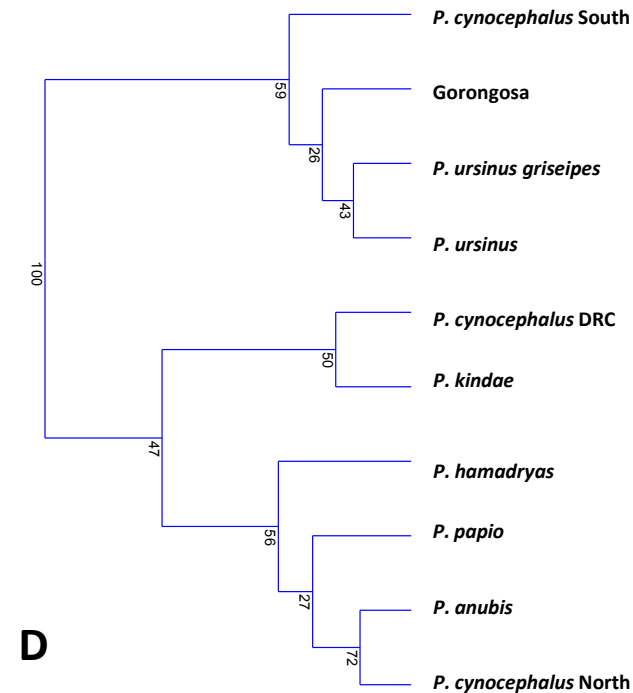
0.12 0.06 0.00



C

Euclidean distance

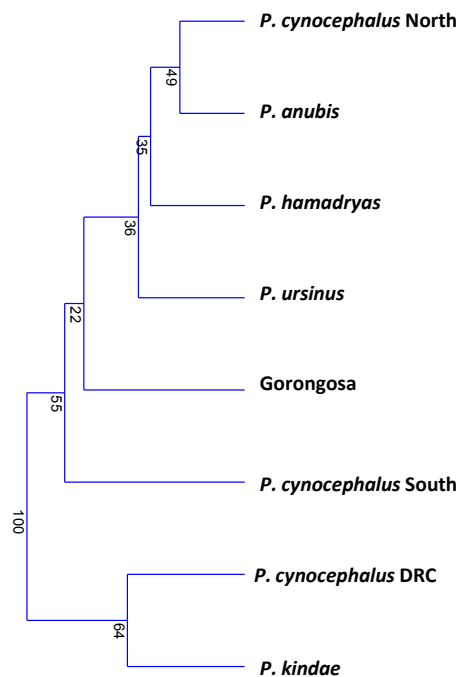
0.12 0.06 0.00



D

Euclidean distance

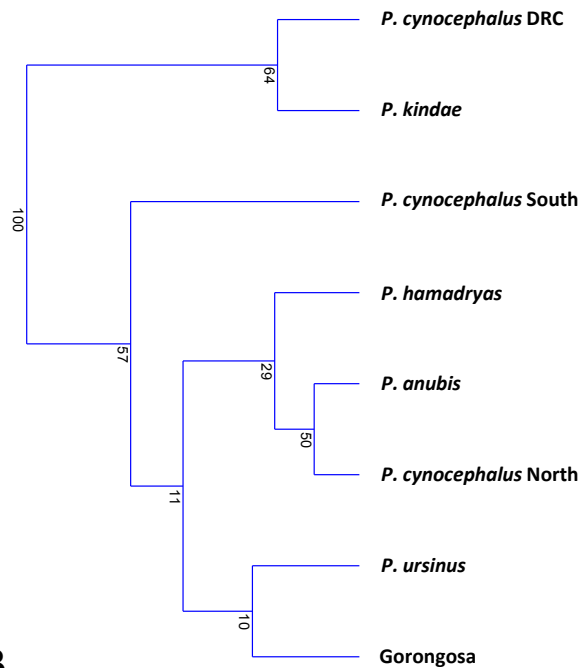
0.12 0.06 0.00



A

Euclidean distance

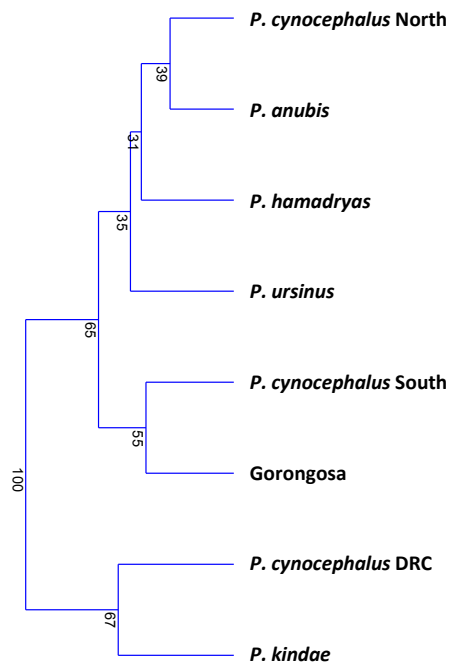
0.12 0.06 0.00



B

Euclidean distance

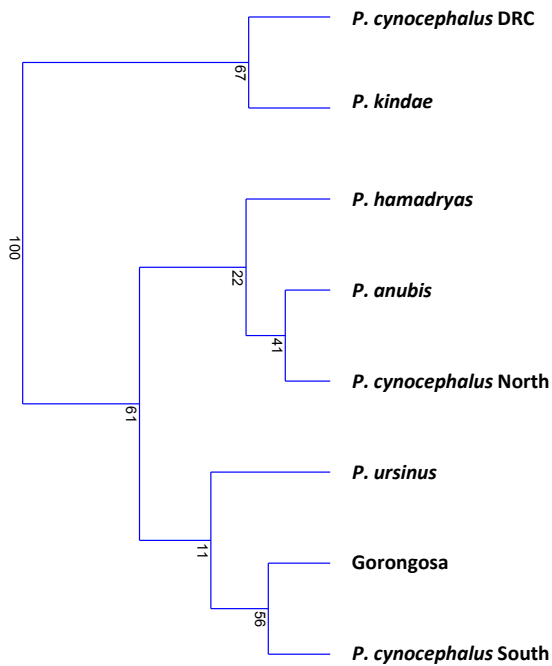
0.12 0.06 0.00



C

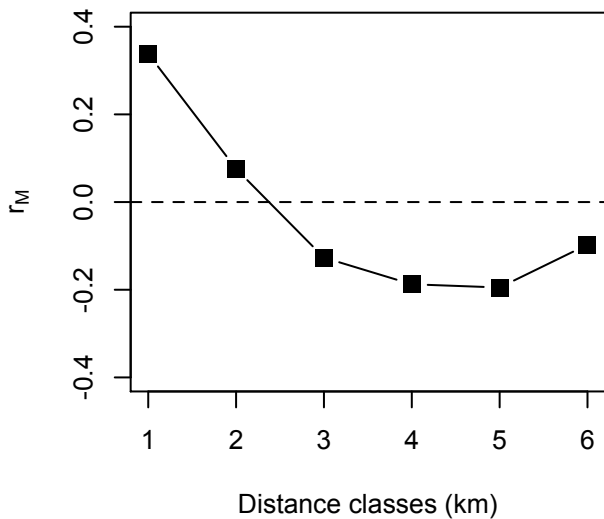
Euclidean distance

0.12 0.06 0.00

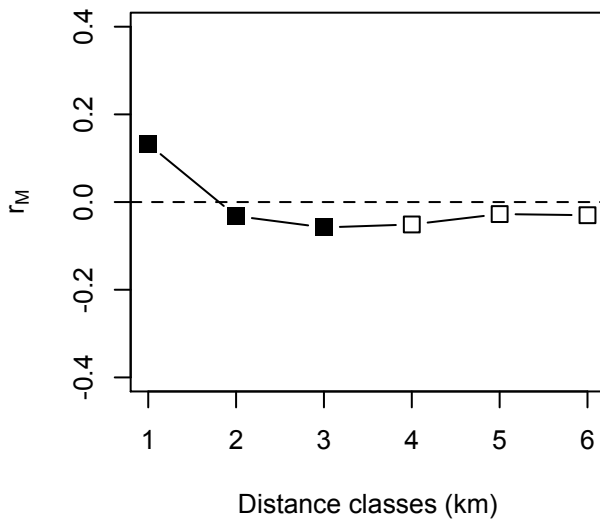


D

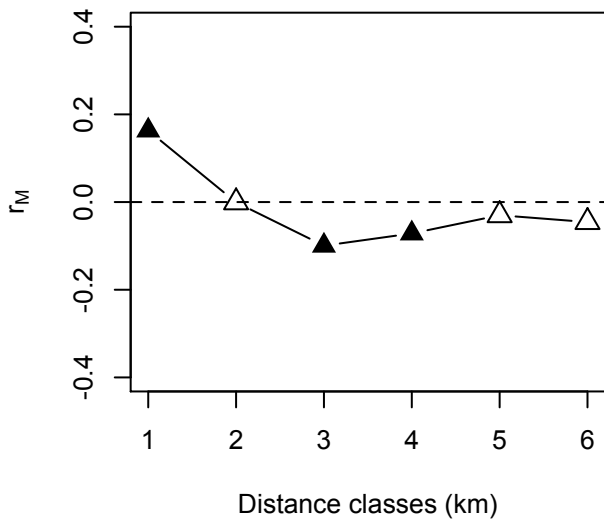
**MT-CYB gene (n=153, all Africa)**



**Craniofacial shape (n=326, all Africa)**



**Craniofacial shape (n=241, males)**



**Craniofacial shape (n=84, females)**

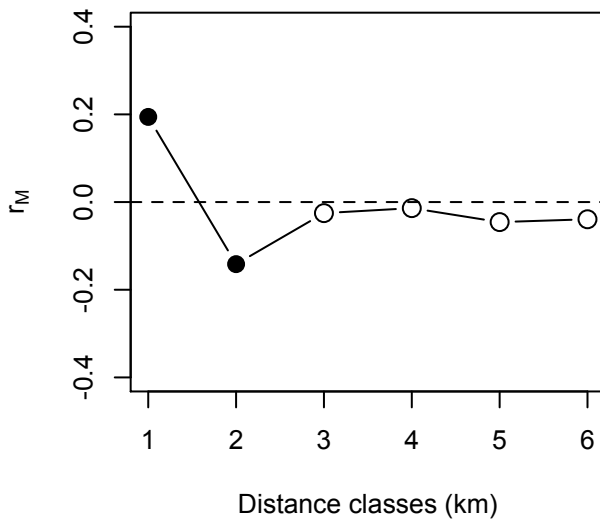


Figure 1. Geographical distribution of baboon species. Map shows the IUCN distribution of hamadryas (*Papio hamadryas*), Guinea (*Papio papio*), olive (*Papio anubis*), yellow (*Papio cynocephalus*), Kinda (*Papio kindae*) and chacma baboons (*Papio ursinus*). Map also shows the distribution of subspecies grayfooted chacma (*Papio ursinus griseipes*), Cape chacma (*P. ursinus ursinus*) and ruacana chacma baboons (*Papio ursinus ruacana*).

Figure 2. Location of GNP in relation to the distribution of baboon species. Map shows the IUCN distribution of yellow and chacma baboons (Hoffmann and Hilton-Taylor, 2008, Kingdon et al., 2016) and the distribution of Luangwa yellow, southern yellow, eastern chacma, northern chacma and southern chacma as estimated by Keller et al. (2010) using mitochondrial DNA clustering. Genetic evidence for hybridization between Kinda and grayfooted chacma has been observed in Kafue National Park (central Zambia; Jolly et al. 2011). In Luangwa National Park (east Zambia; Burrell, 2009) yellow and grayfooted chacma live in close proximity. The Lower Zambezi River is a boundary between grayfooted chacma and yellow baboons.

Figure 3 (a-j). Images depicting the phenotypic diversity of GNP baboons. Numbers correspond to morphological features described in Table 1. Photographs by various members of the PPP team.

Figure 4 (a-f). Images depicting the phenotypic diversity of southern Africa baboons. a) Male Kinda baboon (*P. kindae*) at Mahale Mountains NP, Tanzania (photo by Thomas M. Butynski and Yvonne A. de Jong). b) Male yellow baboon (*P. cynocephalus spp.*) at Quirimbas NP, Mozambique (photo by Daniel Cara). c) Male grayfooted chacma (*P. ursinus griseipes* or *P. ursinus chobiensis*) at Chobe NP, Botswana (photo by Michael

Haworth). d) Female Cape chacma baboons (*P. ursinus ursinus*) at Cape Peninsula (photo by Maria J. Ferrerira da Silva). e) Male grayfooted chacma (*P. ursinus griseipes*) at Okavango Delta, Botswana (photo by John Weir). f) Male Cape chacma (*P. ursinus ursinus*) at Cape Peninsula (photo by Maria J. Ferrerira da Silva).

Figure 5 (a-c). Images depicting the mixed characteristics of an adult male baboon from Gorongosa compared to Malawi and Zimbabwe: a) Yellow baboon (*P. cynocephalus jubilaeus*) at Senga Hills Forest Reserve, Malawi (photo by Jim Auburn). b) Gorongosa baboon (photo by Susana Carvalho). c) Grayfooted chacma (*P. ursinus griseipes*) at Cecil Kop Nature Reserve, Eastern Zimbabwe, located 200 Km west of Gorongosa (photo by Marion Bamford). The face points downward in Gorongosa (b) and grayfooted chacma baboons from Zimbabwe (c), but not in Senga Hills Forest Reserve baboon (a). The color of their hands and feet is similar to their arms in Senga Hills Forest Reserve (a) and Gorongosa (b), but not in grayfooted chacma baboons from Zimbabwe (c).

Figure 6: Principal component plot before size correction. Triangles represent males; circles represent females; colors correspond to groups. (Explained variance: PC1: 45.6%. PC2: 9.9%). The shape changes along the PC1 correspond to an increase/decrease in the projection of the face relative to the braincase. The shape changes along the PC2 correspond to an increase/decrease in klinorhynch (downwardly flexed face).

Figure 7(a-b): Regression score 1 (30.1% of variation explained) and Log Centroid Size plot. a) Males. b) Females.



Figure 8a: Canonical variates plot for males (variance: CV1=30%; CV2=22%). GNP baboons are at one extreme of the distribution, overlapping with *P. ursinus*. The *P. kindae* and *P. cynocephalus* DRC groups cluster together. Beside *P. papio* and *P. kindae/P. cynocephalus* DRC, all other groups are distributed along a continuum. Target wireframe in black color.

Figure 8b: Canonical variates plot for females (variance: CV1=53.8%; CV2=16.2%). CV1 separates *P. kindae/P. cynocephalus* DRC from all other groups. GNP baboons are at one extreme of the distribution along CV2. Target wireframe in black color.

Figure 9a: PCA plot of 'size corrected' mean groups shape for males (PC1=49.9%; PC2=21.5%). Gorongosa baboons cluster together with *P. ursinus*, *P. ursinus griseipes* and *P. cynocephalus* south, while *P. cynocephalus* north, *P. anubis*, *P. hamadryas* and *P. papio* form a different cluster. *P. kindae* falls closer to *P. cynocephalus* DRC and both are apart from other group means. PC1 represents shape changes related to klinorhynch. PC2 represents shape changes related to the breath of the middle face.

Figure 9b: PCA plot of 'size corrected' mean groups shape for females (PC1=48.1%; PC2=21.4%). Gorongosa baboons cluster between *P. ursinus* and *P. cynocephalus* south. PC1 represents shape changes related to the elongation of the face. PC2 represents shape changes related to the breath of the middle face.

Figure 10(a-g). All principal components for male (a-d) and female (e-g) between-groups PCA.

Figure 11. Agglomerative clustering trees for males. UPGMA (a) and Ward's method (b) using all principal components of group means by GPA. UPGMA (c) and Ward's method

(d) excluding one component (PC3: 9.6% explained variance) summarizing most differences between Gorongosa and all other groups in order to control for scanning error.

Figure 12. Agglomerative clustering trees for females. UPGMA (a) and Ward's method (b) using all principal components of group means by GPA. UPGMA (c) and Ward's method (d) excluding one component (PC3: 14.4% explained variance) summarizing most differences between Gorongosa and all other groups in order to control for scanning error.

Figure 13 (a-d). . a) Mantel correlogram for genetic distance. Mantel correlogram shows a pronounced steep pattern, starting with moderate positive correlation in the first distance class (class 1: 0 to 1,109 km;  $r_M=0.338$ ;  $p\text{-value}=0.001$ ) that decreases towards significant negative correlations (see Table 12). b) Mantel correlogram for 'size-corrected' craniofacial shape distance. The 'size-corrected' shape correlogram shows low positive correlation in the first distance class (class 1: 0 to 1,153 km;  $r_M=0.132$ ;  $P\text{ value}=0.001$ ) and a small decrease towards negative correlations, with a flat pattern from 2,306 km (classes 3 to 6) and no statistical significance after 3,459 km (classes 4 to 6; see Table 9). c) Males (see Table 10). d) Females (see Table 11).

**Table 1. External characteristics of GNP baboons compared to yellow and gray- footed chacma baboons (<sup>a</sup>Jolly 1993, <sup>b</sup>Jolly et al. 2011, <sup>c</sup>Alberts et al. 2001, <sup>d</sup>Altmann et al. 1981, <sup>e</sup><http://kennychiou.com/dissertation/> and <sup>f</sup>Swedell 2011).**

	Phenotypic feature	Gorongosa baboons	Gray-footed chacma baboons	Southern Chacma baboons	Yellow baboons	Kinda baboons
<b>1</b>	<b>General color</b>	Yellow-brown to gray-brown	Gray-brown <sup>(a)</sup>	Dark-brown <sup>(a)</sup>	Yellow-brown <sup>(a)</sup>	Yellow-brown <sup>(a)</sup>
<b>2</b>	<b>Color of dorsal hair</b>	Yellow-brown to gray-brown	Drab gray-brown <sup>(b)</sup>	Dark-brown <sup>(a)</sup>	Yellow-brown <sup>(c)</sup>	Yellow-brown <sup>(a, b)</sup>
<b>3</b>	<b>Color of ventral hair</b>	Light, yellow	Lighter <sup>(a)</sup> . Such as back and limbs <sup>(b)</sup>	Dark. Sometimes lighter than dorsal hair <sup>(a)</sup>	Light, yellow <sup>(a, c)</sup>	Light, yellow <sup>(a)</sup>
<b>4</b>	<b>Color of limbs</b>	Lower limbs are lighter than upper	Uniform (in most cases)	Uniform	Uniform (in most cases)	Uniform

limbs						
5	<b>Eyelid skin color</b>	Pink	Pink	Pink	Pink	Pink
6	<b>Circum-orbital skin color</b>	Some individuals (male or female) show pink infra-orbital skin	Dark, except pregnant female <sup>(b)</sup>	Dark	Pink in some populations (e.g. Luangwa, Catapu)	Light pink “spectacles” surrounding eyes <sup>(b)</sup>
7	<b>Hand/foot hair color</b>	Self (like arms) in most individuals	Self (like arms) or gray <sup>(a)</sup>	Dark <sup>(a)</sup>	Self (like arms) <sup>(a)</sup>	Self (like arms) <sup>(a)</sup>
8	<b>Silvery fringe on hands/feet</b>	Present in some individuals	Absent <sup>(a)</sup>	Absent <sup>(a)</sup>	Present <sup>(a)</sup>	Present <sup>(a)</sup>
9	<b>Male Body build</b>	Robust but some individuals are taller and thinner	Robust <sup>(b)</sup>	Robust <sup>(b)</sup>	Taller and thinner. <sup>(b)</sup> (Robust in <i>P.c. jubilaeus</i> ).	Very gracile, long limbed <sup>(b)</sup>

10	Sexual dimorphism	Greater (only observed, not measured)	Greater (adult male 2.0 to 1.9 times adult female) <sup>(b, f)</sup>	Greater (adult male 2.0 to 1.8 times adult female) <sup>(b, e)</sup>	Greater to Smaller (adult male 2.1 to 1.6 times adult female) <sup>(f)</sup>	Smaller (adult male 1.7 to 1.5 times adult female) <sup>(b, e)</sup>
11	Tail shape	Bent in most individuals; high arch in some females	Bent <sup>(a)</sup>	Bent <sup>(a)</sup>	Bent but variable <sup>(a)</sup>	Arched <sup>(a)</sup> or usually high arch <sup>(b)</sup>
12	Facial orientation	Downwardly flexed (increased klinorhynchy)	Downwardly flexed <sup>(a)</sup> (increased klinorhynchy)	Downwardly flexed <sup>(a)</sup> (increased klinorhynchy)	“Normal” <sup>(a)</sup> (less klinorhynchy)	“Normal” <sup>(a)</sup> (less klinorhynchy)
13	Natal Coat	Black	Black <sup>(a, b)</sup>	Black <sup>(a)</sup>	Black <sup>(a)</sup>	White <sup>(b)</sup>
14	Infant-2 <sup>(d)</sup> hair color	Yellow, lighter than adults. (In transition Inf.1-2, black spots in tail and head remain longest).	Brown to cream- colored.	Dark-brown.	Brown to cream- colored, often lighter than adults. (In transition 1-2, black spots in tail and	Brown to cream- colored. <sup>(e)</sup>

shoulders remain

longest).<sup>(d)</sup>

---

**Table 2. Morphotypes composition in the morphometrics sample (including *P. cynocephalus* geographic subdivision).**

	Males	Females	N
<i>P. anubis</i>	112	43	155
<i>P. cynocephalus</i>	40	21	61
<i>P. cynocephalus north</i>	(31)	(15)	(46)
<i>P. cynocephalus south</i>	(4)	(2)	(6)
<i>P. cynocephalus DRC</i>	(5)	(4)	(9)
<i>P. hamadryas</i>	31	8	39
<i>P. kindae</i>	10	7	17
<i>P. papio</i>	12	1	13
<i>P. ursinus</i>	51	12	63
<i>P. ursinus griseipes</i>	4	0	4
Gorongosa	7	4	11
Total	267	96	363

**Table 3: Anatomical definitions of the forty-three, three-dimensional landmarks used in this study (defined in: Dunn et al., 2013 and Cardini et al., 2007; \* defined in this study)**

N°	Description
1	Prosthion: antero-inferior point on projection of pre-maxilla between central incisors
2	Prosthion2: antero-inferior-most point on pre-maxilla, equivalent to prosthion but between central and lateral incisors
3	Anterior-most point of canine alveolus
4	Mesial P3: most mesial point on P3 alveolus, projected onto alveolar margin
5-8	Contact points between adjacent pre-molars/molars, projected labially onto alveolar margin
9	Posterior midpoint onto alveolar margin of M3
10-13	Contact points between adjacent pre-molars/molars, projected lingually onto alveolar margin
14*	Anterior-most point of incisive foramen
15*	Middle-line point of the incisive foramen projected onto its margin
16	Posterior-most point of incisive foramen
17	Greater palatine foramen
18	Point of maximum curvature on the posterior edge of the palatine
19	Tip of posterior nasal spine
20-21	Anterior and posterior tip of the external auditory meatus
22	Inion: most posterior point of the cranium
23	Most lateral meeting point of mastoid part of temporal bone and supraoccipital
24	Nasospinale: inferior-most midline point of piriform aperture
25	Point corresponding to largest width of piriform aperture
26	Meeting point of nasal and pre-maxilla on margin of piriform aperture
27	Rhinion: most anterior midline point on nasals
28	Nasion: midline point on fronto-nasal suture
29	Glabella: most forward projecting midline point of frontals at the level of the supraorbital ridges
30	Supraorbital notch
31	Frontomale orbitale: where frontozygomatic suture crosses inner orbital rim



- 32 Zygo-max superior: antero-superior point of zygomaticomaxillary suture taken at orbit rim
  - 33 Center of nasolacrimal foramen (fossa for lacrimal duct)
  - 34 Frontomalare temporale: where frontozygomatic suture crosses lateral edge of zygoma
  - 35 Maximum curvature of anterior upper margin of zygomatic arch
  - 36 Zygo-temp superior: superior point of zygomaticotemporal suture on lateral face of zygomatic arch
  - 37 Zygo-temp inferior: infero-lateral point of zygomaticotemporal suture on lateral face of zygomatic arch
  - 38 Posterior-most point on curvature of anterior margin of zygomatic process of temporal bone
  - 39 Articular tubercle
  - 40 Distal-most point on post-glenoid process
  - 41 Posterior-most point of zygomatic process of temporal bone
  - 42 Bregma: junction of coronal and sagittal sutures
  - 43 Lambda: junction of sagittal and lamboid sutures
-

Table 4. Results from the discriminant function analysis of pairs of groups (males) before correcting for size: Procrustes distances among groups (P-values from 1,000 permutation test rounds). Significant results at <0.05 are shown in bold. Not significant results are shown in gray.

Males									
	Gorongosa	<i>P. anubis</i>	<i>P. c. DRC</i>	<i>P. c. north</i>	<i>P. c. south</i>	<i>P. hamadryas</i>	<i>P. kindae</i>	<i>P. papio</i>	<i>P. ursinus</i>
	<b>0.0578</b>								
<i>P. anubis</i>	( <b>&lt;0.001</b> )								
	<b>0.1518</b>	<b>0.1304</b>							
<i>P. cynocephalus DRC</i>	( <b>&lt;0.001</b> )	( <b>&lt;0.001</b> )							
	<b>0.0582</b>	<b>0.2697</b>	<b>0.1146</b>						
<i>P. cynocephalus north</i>	( <b>&lt;0.001</b> )	( <b>&lt;0.001</b> )	( <b>&lt;0.001</b> )						
	<b>0.0489</b>	<b>0.0413</b>	<b>0.1256</b>	0.0320					
<i>P. cynocephalus south</i>	( <b>0.005</b> )	( <b>0.007</b> )	<b>0.006</b>	(0.298)					

	<b>0.0817</b>	<b>0.0438</b>	<b>0.0991</b>	<b>0.0392</b>	<b>0.0568</b>				
<i>P. hamadryas</i>	<b>(&lt;0.001)</b>	<b>(&lt;0.001)</b>	<b>(&lt;0.001)</b>	<b>(&lt;0.001)</b>	<b>(&lt;0.001)</b>				
	<b>0.1379</b>	<b>0.1183</b>	<b>0.0031</b>	<b>0.1008</b>	<b>0.1122</b>	<b>0.0887</b>			
<i>P. kindae</i>	<b>(&lt;0.001)</b>	<b>(&lt;0.001)</b>	<b>0.1860</b>	<b>(&lt;0.001)</b>	<b>(&lt;0.001)</b>	<b>(&lt;0.001)</b>			
	<b>0.0879</b>	<b>0.0569</b>	<b>0.0927</b>	<b>0.0501</b>	<b>0.0665</b>	<b>0.0412</b>	<b>0.0846</b>		
<i>P. papio</i>	<b>(&lt;0.001)</b>	<b>(&lt;0.001)</b>	<b>(&lt;0.001)</b>	<b>(&lt;0.001)</b>	<b>(0.001)</b>	<b>(&lt;0.001)</b>	<b>(&lt;0.001)</b>		
	<b>0.0407</b>	<b>0.0390</b>	<b>0.1412</b>	<b>0.0362</b>	<b>0.0313</b>	<b>0.0651</b>	<b>0.1272</b>	<b>0.0740</b>	
<i>P. ursinus</i>	<b>(&lt;0.001)</b>	<b>(&lt;0.001)</b>	<b>(&lt;0.001)</b>	<b>(&lt;0.001)</b>	<b>(0.165)</b>	<b>(&lt;0.001)</b>	<b>(&lt;0.001)</b>	<b>(&lt;0.001)</b>	
	<b>0.04378</b>	<b>0.0437</b>	<b>0.1472</b>	<b>0.0438</b>	<b>0.0401</b>	<b>0.0711</b>	<b>0.1325</b>	<b>0.0814</b>	<b>0.0242</b>
<i>P. ursinus griseipes</i>	<b>(0.1390)</b>	<b>0.003</b>	<b>(0.007)</b>	<b>(0.037)</b>	<b>(0.275)</b>	<b>(&lt;0.001)</b>	<b>(0.001)</b>	<b>(0.001)</b>	<b>(0.695)</b>

Table 5. Results from the discriminant function analysis of pairs of groups (females) before correcting for size: Procrustes distances among groups (P-values from 1,000 permutation test rounds). Significant results at <0.05 are shown in bold. Not significant results are shown in gray.

Females ( <i>P. papio</i> and <i>P. cynocephalus</i> south are excluded due to small sample size)						
	Gorongosa	<i>P. anubis</i>	<i>P. c. DRC</i>	<i>P. c. north</i>	<i>P. hamadryas</i>	<i>P. kindae</i>
	<b>0.0466</b>					
<i>P. anubis</i>	<b>(0.002)</b>					
	<b>0.1175</b>	<b>0.1234</b>				
<i>P. cynocephalus DRC</i>	<b>(0.004)</b>	<b>(&lt;0.001)</b>				
	<b>0.0448</b>	<b>0.0249</b>	<b>0.1076</b>			
<i>P. cynocephalus north</i>	<b>(0.025)</b>	<b>(0.004)</b>	<b>(&lt;0.001)</b>			
	<b>0.0475</b>	<b>0.0277</b>	<b>0.109</b>	0.0278		
<i>P. hamadryas</i>	<b>(0.038)</b>	<b>(0.042)</b>	<b>(0.002)</b>	(0.199)		
<i>P. kindae</i>	<b>0.1035</b>	<b>0.1104</b>	0.0334	<b>0.0940</b>	<b>0.0962</b>	

	(0.002)	(<0.001)	(0.423)	(<0.001)	(<0.001)	
	0.0431	<b>0.0276</b>	<b>0.1252</b>	<b>0.0317</b>	0.0348	<b>0.1127</b>
<i>P. ursinus</i>	(0.078)	<b>(0.004)</b>	<b>(&lt;0.001)</b>	<b>(0.03)</b>	(0.055)	<b>(&lt;0.001)</b>

**Table 6. Results from the discriminant function analysis of pairs of groups (males) after correcting for size: Procrustes distances among groups (P-values from 1,000 permutation test rounds). Significant results at <0.05 are shown in bold. Not significant results are shown in gray.**

<b>Males</b>									
	Gorongosa	<i>P. anubis</i>	<i>P. c. DRC</i>	<i>P. c. north</i>	<i>P. c. south</i>	<i>P. hamadryas</i>	<i>P. kindae</i>	<i>P. papio</i>	<i>P. ursinus</i>
	<b>0.0568</b>								
<i>P. anubis</i>	<b>(&lt;0.001)</b>								
	<b>0.0850</b>	<b>0.0582</b>							
<i>P. cynocephalus DRC</i>	<b>(&lt;0.001)</b>	<b>(&lt;0.001)</b>							
	<b>0.0517</b>	<b>0.0217</b>	<b>0.0582</b>						
<i>P. cynocephalus north</i>	<b>(&lt;0.001)</b>	<b>(&lt;0.001)</b>	<b>(&lt;0.001)</b>						
	<b>0.0452</b>	<b>0.0413</b>	<b>0.0688</b>	0.0314					
<i>P. cynocephalus south</i>	<b>(0.070)</b>	<b>(0.003)</b>	<b>(0.021)</b>	(0.135)					

	<b>0.0694</b>	<b>0.0286</b>	<b>0.0542</b>	<b>0.0357</b>	<b>0.0520</b>				
<i>P. hamadryas</i>	<b>(&lt;0.001)</b>	<b>(&lt;0.001)</b>	<b>(&lt;0.001)</b>	<b>(&lt;0.001)</b>	<b>(&lt;0.001)</b>				
	<b>0.0731</b>	<b>0.0490</b>	0.0320	<b>0.0446</b>	<b>0.0564</b>	<b>0.0483</b>			
<i>P. kindae</i>	<b>(&lt;0.001)</b>	<b>(&lt;0.001)</b>	(0.145)	<b>(&lt;0.001)</b>	<b>(0.004)</b>	<b>(&lt;0.001)</b>			
	<b>0.0667</b>	<b>0.0301</b>	<b>0.0622</b>	<b>0.0401</b>	<b>0.0557</b>	<b>0.0385</b>	<b>0.0597</b>		
<i>P. papio</i>	<b>(&lt;0.001)</b>	<b>(&lt;0.001)</b>	<b>(&lt;0.001)</b>	<b>(&lt;0.001)</b>	<b>(&lt;0.001)</b>	<b>(&lt;0.001)</b>	<b>(&lt;0.001)</b>		
	<b>0.0402</b>	<b>0.0387</b>	<b>0.0725</b>	<b>0.0290</b>	0.0283	<b>0.0527</b>	<b>0.0596</b>	<b>0.0592</b>	
<i>P. ursinus</i>	<b>(&lt;0.001)</b>	<b>(&lt;0.001)</b>	<b>(&lt;0.001)</b>	<b>(&lt;0.001)</b>	(0.172)	<b>(&lt;0.001)</b>	<b>(&lt;0.001)</b>	<b>(&lt;0.001)</b>	
	0.0434	<b>0.0422</b>	<b>0.0730</b>	0.0336	0.034	<b>0.0553</b>	<b>0.0586</b>	<b>0.0591</b>	0.0232
<i>P. ursinus griseipes</i>	(0.092)	<b>(0.008)</b>	<b>(0.023)</b>	(0.059)	(0.459)	<b>(0.001)</b>	<b>(0.001)</b>	<b>(&lt;0.001)</b>	(0.640)

**Table 7. Results from the discriminant function analysis of pairs of groups (females) after correcting for size: Procrustes distances among groups (P-values from 1,000 permutation test rounds). Significant results at <0.05 are shown in bold. Not significant results are shown in gray.**

<b>Females (<i>P. papio</i> and <i>P. cynocephalus</i> south are excluded due to small sample size)</b>						
	Gorongosa	<i>P. anubis</i>	<i>P. c. DRC</i>	<i>P. c. north</i>	<i>P. hamadryas</i>	<i>P. kindae</i>
	<b>0.0454</b>					
<i>P. anubis</i>	<b>(&lt;0.001)</b>					
	<b>0.0637</b>	<b>0.0600</b>				
<i>P. cynocephalus DRC</i>	<b>(0.033)</b>	<b>(&lt;0.001)</b>				
	<b>0.0439</b>	<b>0.0180</b>	<b>0.0584</b>			
<i>P. cynocephalus north</i>	<b>(0.007)</b>	<b>(0.022)</b>	<b>(&lt;0.001)</b>			
	<b>0.0471</b>	0.0234	<b>0.0585</b>	0.0289		
<i>P. hamadryas</i>	<b>(0.009)</b>	(0.055)	<b>(0.004)</b>	(0.06)		
<i>P. kindae</i>	<b>0.05773</b>	<b>0.0559</b>	0.0326	<b>0.0523</b>	<b>0.0555</b>	



	( <b>&lt;0.001</b> )	( <b>&lt;0.001</b> )	(0.401)	( <b>&lt;0.001</b> )	( <b>0.001</b> )	
	0.0426	<b>0.0282</b>	<b>0.0659</b>	<b>0.0289</b>	<b>0.0315</b>	<b>0.0636</b>
<i>P. ursinus</i>	(0.008)	( <b>&lt;0.001</b> )	( <b>&lt;0.001</b> )	( <b>0.015</b> )	( <b>0.046</b> )	( <b>&lt;0.001</b> )

**Table 8. Classification and misclassification DFA cross-validations for males *P. u. griseipes* /*P. cynocephalus* south, before and after size correction (reliability of the discrimination is assessed by leave-one-out cross-validation).**

Allocated to			
(before size correction)			
	<i>P. u. griseipes</i>	<i>P. c. south</i>	Total
<i>P. u. griseipes</i>	2	2	4
<i>P. c. south</i>	4	0	4
(after size correction)			
<i>P. u. griseipes</i>	2	2	4
<i>P. c. south</i>	4	0	4

**Table 9. Mantel correlogram results for “size corrected” shape and geographic distances with 999 permutations.**

Overall Mantel statistic $r$ ( $r_M$ )= 0.121; significance: 0.001				
Class	Distance range (km)	$r_M$	P value	Bonf. Correc.
1	0 – 1,153	0.132	0.001	0.001
2	1,153 – 2,306	-0.032	0.02	0.04
3	2,306 – 3,459	-0.058	0.002	0.006
4	3,459 – 4,612	-0.051	0.013	0.052
5	4,612 – 5,765	-0.027	0.121	0.605
6	5,765 – 6,918	-0.030	0.075	0.450

**Table 10. Mantel correlogram results for male “size corrected” shape and geographic distances with 999 permutations.**

<b>Overall Mantel statistic <math>r</math> (<math>r_M</math>)= 0.161; significance: 0.001</b>				
<b>Class</b>	<b>Distance range (km)</b>	<b><math>r_M</math></b>	<b>P value</b>	<b>Bonf. Correc.</b>
1	0 – 1,141	0.163	0.001	0.001
2	1,141 – 2,282	-0.000	0.460	0.920
3	2,282 – 3,423	-0.099	0.001	0.003
4	3,423 – 4,564	-0.071	0.006	0.024
5	4,564 – 5,706	-0.030	0.120	0.600
6	5,706 – 6,848	-0.045	0.059	0.354

**Table 11. Mantel correlogram results for female “size corrected” shape and geographic distances with 999 permutations.**

Overall Mantel statistic $r$ ( $r_M$ )= 0.152; significance: 0.021				
Class	Distance range (km)	$r_M$	P value	Bonf. Correc.
1	0 – 1,125	0.194	0.001	0.001
2	1,125 – 2,251	-0.141	0.002	0.004
3	2,251 – 3,377	-0.025	0.249	0.747
4	3,377 – 4,502	-0.013	0.338	1.352
5	4,502 – 5,628	-0.045	0.129	0.645
6	5,628 – 6,755	-0.039	0.194	1.164

**Table 12. Mantel correlogram results for genetic (CYT-B gene) and geographic distances with 999 permutations.**

Overall Mantel statistic $r$ ( $r_M$ )= 0.411; significance: 0.001				
Class	Distance range (km)	$r_M$	P value	Bonf. Correc.
1	0 – 1,109	0.338	0.001	0.001
2	1,109 – 2,218	0.076	0.001	0.002
3	2,218 – 3,327	-0.127	0.001	0.003
4	3,327 – 4,436	-0.188	0.001	0.004
5	4,436 – 5,545	-0.194	0.001	0.005
6	5,545 – 6,655	-0.097	0.001	0.006